NATIONAL ADVISORY COMMITTEE FOR AERONAUTICS

TECHNICAL NOTE 2175

EFFECT OF AN UNSWEPT WING ON THE CONTRIBUTION OF UNSWEPT-TAIL CONFIGURATIONS TO THE LOW-SPEED STATIC- AND ROLLING-STABILITY DERIVATIVES OF A MIDWING AIRPLANE MODEL

By William Letko and Donald R. Riley

Langley Aeronautical Laboratory
Langley Air Force Base, Va.

NACA

Washington
August 1950

NATIONAL ADVISORY COMMITTEE FOR AERONAUTICS

TECHNICAL NOTE 2175

EFFECT OF AN UNSWEPT WING ON THE CONTRIBUTION OF UNSWEPT-TAIL CONFIGURATIONS TO THE LOW-SPEED STATIC- AND ROLLING-STABILITY DERIVATIVES OF A MIDWING AIRPLANE MODEL

By William Letko and Donald R. Riley

SUMMARY

An investigation has been conducted in the Langley stability tunnel to determine the effect of an unswept wing on the contribution of unswept-tail configurations to the low-speed static- and rolling-stability derivatives of a midwing airplane model.

The results of the investigation show that, at angles of attack almost to the angle of maximum lift, there are only small differences in the tail contributions to the static-lateral-stability derivatives for configurations with wing on and with wing off. For this range of angles of attack the contributions of the vertical tail can be estimated fairly accurately by the available procedures.

The available procedures generally predict the wing-off values of the rolling derivatives at low angles of attack with reasonable accuracy. Altering these equations to account for sidewash caused by the unsymmetrical wing load (due to roll) brings the calculated wing-on values into much better agreement with the measured wing-on values.

Some error in the estimated contribution of the tail to the yawing moment caused by roll results for the low-horizontal-tail configuration because of a forward shift in the center of pressure of the vertical tail caused by the horizontal tail.

INTRODUCTION

Recent advances in the understanding of the principles of high-speed flight have led to significant changes in the design of component parts of airplanes. In many instances consideration is given to configurations

which are beyond the range covered by available design information regarding stability characteristics. The effects of changes in wing design on stability characteristics have been extensively investigated. In order to provide information on the influence of other parts of the complete airplane, an investigation of a model having various interchangeable parts is being conducted in the Langley stability tunnel. Reference 1 presents the results of an investigation on the effect of horizontal-tail location on the low-speed static lateral stability characteristics of a model having 45° sweptback wing and tail surfaces.

As part of this general investigation, the effect of an unswept wing on the contribution of an unswept vertical tail to the static lateral and rolling stability characteristics has been determined, and the results are presented herein. These results serve the purpose of checking the validity of present methods of estimating the contributions of component parts of airplanes when applied to representative current high-speed airplane designs.

SYMBOLS

The data presented herein are in the form of standard NACA coefficients of forces and moments which are referred to the stability system of axes with the origin coinciding with the wing aerodynamic center. The positive directions of the forces, moments, and angular displacements are shown in figure 1. The coefficients and symbols are defined as follows:

C_L	lift coefficient $\left(L/qS_W\right)$
C_X	longitudinal-force coefficient $\left(X/qS_W\right)$
C_Y	lateral-force coefficient $\left(Y/qS_W\right)$
C_l	rolling-moment coefficient $\left(L'/qS_Wb\right)$
C_m	pitching-moment coefficient $\left(M/qS_W\bar{c}\right)$
C_n	yawing-moment coefficient $\left(N/qS_Wb\right)$
L	lift
X	longitudinal force (-Drag at $\psi = 0^\circ$)
Y	lateral force

L'	rolling moment
M	pitching moment
N	yawing moment
q	dynamic pressure
S_W	wing area
S_V	vertical-tail area
b	wing span
A	aspect ratio
c	wing chord
$\bar{c}$	wing mean aerodynamic chord
h	vertical distance above or below tunnel center line
z	perpendicular distance from fuselage center line to center of pressure of vertical tail
l_V	tail length; distance, parallel to fuselage center line, from wing mounting point to center of pressure of vertical tail
α	angle of attack of wing or fuselage center line
α_V	angle of attack of vertical tail measured in a horizontal plane, positive when it results in a positive lateral force
ψ	angle of yaw
σ	sidewash angle at vertical tail; the change in angle of attack of a section of vertical tail resulting from addition of a wing to fuselage and vertical-tail combination operating in rolling condition, positive when it results in a positive lateral force
V	free-stream velocity
p	rolling angular velocity

$\frac{\partial \alpha_V}{\partial \frac{pb}{2V}}$ rate of change of vertical-tail angle of attack with wing-tip helix angle

$\frac{\partial \sigma}{\partial \frac{pb}{2V}}$ rate of change of sidewash angle at vertical tail with wing-tip helix angle

$\frac{pb}{2V}$ wing-tip helix angle

C_{L_α} lift-curve slope of wing

$C_{L_{\alpha_V}}$ lift-curve slope of vertical tail (C_L of vertical tail based on vertical-tail area)

$C_{Y_\psi} = \frac{\partial C_Y}{\partial \psi}$

$C_{n_\psi} = \frac{\partial C_n}{\partial \psi}$

$C_{l_\psi} = \frac{\partial C_l}{\partial \psi}$

$C_{Y_p} = \frac{\partial C_Y}{\partial \frac{pb}{2V}}$

$C_{n_p} = \frac{\partial C_n}{\partial \frac{pb}{2V}}$

$C_{l_p} = \frac{\partial C_l}{\partial \frac{pb}{2V}}$

APPARATUS AND MODELS

The tests were made in the 6-foot-diameter test section of the Langley stability tunnel. This section is equipped with a motor-driven rotor which imparts a twist to the air stream so that a model mounted rigidly in the tunnel is in a field of flow similar to that which exists about an airplane in rolling flight (reference 2).

The model used for the present investigation was designed to permit tests of wing alone, fuselage alone, or the fuselage in combination with any of several tail configurations with or without the wing. The fuselage used in the investigation was a body of revolution which had a circular-arc nose and a blunt-tail cone. Two horizontal-tail positions were tested, one located on the fuselage center line and the other located at a position approximately two-thirds the height of the vertical tail. A list of the geometric characteristics of various component parts is given in the following table:

Fuselage:	
Length, inches	40.0
Fineness ratio	6.67
Wing:	
Aspect ratio	4.0
Taper ratio	0.6
Quarter-chord sweep angle, degrees	0
Incidence, degrees	0
Dihedral angle, degrees	0
Twist, degrees	0
Airfoil section	NACA 65A008
Area, square inches	324
Span, inches	36
Mean aerodynamic chord, inches	9.19
Vertical tail:	
Aspect ratio	2.0
Taper ratio	0.6
Quarter-chord sweep angle, degrees	0
Airfoil section	NACA 65A008
Area, square inches	48.60
Span, inches	9.86
Mean aerodynamic chord, inches	5.03
Tail length, inches	15.38

Horizontal tail:

Aspect ratio	4.0
Taper ratio	0.6
Quarter-chord sweep angle, degrees	0
Incidence, degrees	0
Dihedral angle, degrees	0
Twist, degrees	0
Airfoil section	NACA 65A008
Area, square inches	64.80
Span, inches	16.10
Mean aerodynamic chord, inches	4.11

Details of the wing, fuselage, and tail surfaces and the relative locations of the wing and tails with respect to the fuselage are given in figure 2. A photograph of one of the configurations mounted in the tunnel is given as figure 3.

The test configurations and designations used in identifying the data in the figures are given in the following table:

Wing	W
Fuselage	F
Fuselage with vertical tail	F + V
Fuselage with vertical tail and low horizontal tail	F + V + H_L
Fuselage with vertical tail and high horizontal tail	F + V + H_H
Wing with fuselage	W + F
Wing with fuselage and vertical tail	W + F + V
Wing with fuselage, vertical tail, and low horizontal tail	W + F + V + H_L
Wing with fuselage, vertical tail, and high horizontal tail	W + F + V + H_H

For the tests the model was mounted on a single strut support at the quarter-chord point of the wing which coincided with the 50-percent point of the fuselage length (fig. 2). Forces and moments were measured by means of a conventional six-component balance system.

TESTS

Tests were made at a dynamic pressure of 39.8 pounds per square foot, which corresponds to a Mach number of about 0.166 and a Reynolds number of 8.8×10^5 based on the mean aerodynamic chord of the wing.

The model was tested through an angle-of-attack range from about -4° up to and beyond the angle of maximum lift at angles of yaw of 0° and $\pm 5^\circ$

in straight flow and at an angle of yaw of 0° in rolling flow. For the straight-flow tests at 0° angle of yaw, lift, drag, and pitching moments are presented. Data obtained in straight flow at ±5° yaw and in rolling flow at several values of $pb/2V$ were used to obtain derivatives of lateral force, yawing moment, and rolling moment with respect to yaw angle and wing-tip helix angle. The test values of $pb/2V$ were ±0.0206, ±0.0411, and ±0.0616. Also for these values of $pb/2V$ sidewash angles in the plane of symmetry behind the isolated wing were determined by means of a yaw tube. The sidewash measurements were made at 0, 3, 6, and 9 inches vertically above and below the tunnel center line. The measurements were made at two longitudinal positions; one was 1.28 feet $\left(\frac{l_V}{b} = 0.427\right)$ behind the wing-mounting point (corresponding to the longitudinal position of the center of pressure of the vertical tail at zero angle of attack of the model) and the other was at about twice that distance or 2.56 feet $\left(\frac{l_V}{b} = 0.854\right)$. For the position 1.28 feet behind the wing-mounting point, measurements were made at 0°, 4°, 8°, and 12° angle of attack of the wing, whereas for the other longitudinal position, measurements were only made at an angle of attack of the wing of 0°.

CORRECTIONS

The angle of attack, longitudinal-force coefficient, pitching-moment coefficient, and rolling-moment coefficient have been corrected for the effects of the jet boundaries. The data are not corrected for blocking, turbulence, or support-strut interference.

RESULTS AND DISCUSSION

Presentation of Results

The results of the present investigation are presented in figures 4 to 16. The static longitudinal and lateral stability characteristics and the rolling stability characteristics of the basic configurations are presented in figures 4 to 8. Figures 9 to 16 are used to facilitate the analysis of the data and include sidewash measurements mentioned under tests. The analysis has been treated as follows.

First, some of the characteristics of the complete airplane configurations are given. (It should be pointed out that only a brief analysis of the complete configuration is presented and no detailed analysis of the longitudinal stability characteristics is given for any configuration.)

Second, the characteristics of the component parts of the airplane are discussed, with most emphasis being placed on the wing-on and wing-off contribution of the tail group to the static- and rolling-stability derivatives.

All tail increments were obtained from the measurements in the manner illustrated:

Case 1, wing off:

For the horizontal tail off

$$\Delta C_{n_\psi} = C_{n_{\psi_{F+V}}} - C_{n_{\psi_F}}$$

and for the horizontal tail on

$$\Delta C_{n_\psi} = C_{n_{\psi_{F+V+H}}} - C_{n_{\psi_F}}$$

Case 2, wing on:

For the horizontal tail off

$$\Delta C_{n_\psi} = C_{n_{\psi_{W+F+V}}} - C_{n_{\psi_{W+F}}}$$

and for the horizontal tail on

$$\Delta C_{n_\psi} = C_{n_{\psi_{W+F+V+H}}} - C_{n_{\psi_{W+F}}}$$

It should be noted that when a horizontal tail is used, the tail contribution is considered to consist of the effect of the complete tail group.

Complete Configuration

The lift, longitudinal-force, and pitching-moment characteristics of the complete configurations are presented in figure 4(a). The configuration with the horizontal tail in the low position has a higher maximum lift coefficient than the configuration with the horizontal tail in the high position. The low tail, evidently, is strongly affected by the wing downwash, since the pitching moments are unstable for the assumed center-of-gravity position. The results show that, if the center of gravity of the configuration with the low horizontal tail were adjusted to give the same pitching-moment slope at low angles of attack as that of the configuration with high horizontal tail, the general shape of the

pitching-moment curve would be more satisfactory for the configuration with horizontal tail in the low position. The hypothesis that the effects obtained with the low horizontal tail are caused by the wing and, therefore, are obviously wing-wake effects is confirmed by noting from figure 4(b) that the wing-off lift and pitching-moment characteristics of both tail configurations are about the same.

The variation of the static lateral-stability derivatives C_{Y_ψ}, C_{n_ψ}, and C_{l_ψ} with angle of attack for the complete configurations are given in figure 5. In general, the results were about as were expected. The high horizontal tail slightly reduced the effectiveness of the vertical tail with regard to C_{Y_ψ} and C_{n_ψ}. The horizontal tail in the low position increased both C_{Y_ψ} and C_{n_ψ} but, at the same time, reduced C_{l_ψ} at low angles of attack. A similar result was obtained in reference 1.

The variations of the rolling-stability derivatives C_{Y_p} and C_{n_p} for the complete configurations are much as would be expected (fig. 6) but the variation of C_{l_p} is less linear than usual; however, C_{l_p} is primarily a function of the wing characteristics.

Some differences in the static-lateral- and in the rolling-stability derivatives have been obtained for the two tail configurations, wing on and wing off, which will be discussed subsequently in the section on tail contribution.

Wing Characteristics

The lift, longitudinal-force, and pitching-moment data of the wing alone (fig. 4(a)) show no unusual characteristics. The experimental lift-curve slope is 0.0630, which compares well with the theoretical value of 0.0642 given in reference 3. At low angles of attack the aerodynamic center of the wing is located at about 21.8 percent of the mean aerodynamic chord as compared with the theoretical location which is given in reference 3 as 25 percent of the wing mean aerodynamic chord.

The static-stability derivatives of the wing are plotted against lift coefficient in figure 7 and are compared with values calculated by the methods of reference 4. In general, the calculations are in good agreement with the measured values except at high lift coefficients.

The values of the wing rolling derivatives are plotted against lift coefficient in figure 8 and are compared with calculated values. The

values of C_{n_p} calculated by the method of reference 5 agree very well with the measured values at low lift coefficients. At high lift coefficients, although the calculations show the correct trends, the values of C_{n_p} are overestimated. The fact that the method of reference 5 overestimates the values of C_{n_p} for low-aspect-ratio wings of small sweep has been previously noted in other investigations.

Also in figure 8 is a comparison of the experimental values of C_{l_p} with those calculated by the method of reference 6. The values at zero lift agree quite well, but the experimental values show a rapid increase of C_{l_p} when the lift coefficient is increased, whereas the calculated values are almost constant for low and medium lift coefficients. This nonlinear variation of measured C_{l_p} results even though the lift-curve slope of the wing appears to be linear over this range of lift coefficient. This variation may be the result of local increases of the lift-curve slope of the tip sections, which are significant in determining the C_{l_p} of the wing, together with decreases of the lift-curve slope of the midspan sections, which are relatively unimportant in their effect on C_{l_p}.

The derivative C_{Y_p} is small and increases almost linearly with lift coefficient (fig. 8); however, the rate of increase with lift coefficient is somewhat less than the empirical result found in reference 5. Figure 9 of reference 5 indicates that C_{Y_p}/C_L is proportional to $1/A$ for unswept wings.

Fuselage Characteristics

Although the fuselage contributes somewhat to most of the aerodynamic forces and moments, the most important effects on the aerodynamic characteristics of the airplane are caused by the contribution of the fuselage to the static longitudinal and directional stability. The fuselage contributes an unstable moment both in pitch and yaw. As can be seen from figure 4(b), the instability in pitch decreases as the angle of attack is increased, whereas the instability in yaw, measured at small angles of yaw, remains practically constant throughout the angle-of-attack range (fig. 5(b)). The instability of this fuselage is very nearly the same as that of the fuselage reported on in reference 1, with the exception that the fuselage of reference 1 is more unstable in pitch at high angles of attack. (The fuselages are of the same length, are identical ahead of the midpoint, and differ only in the shape of the tail cone. The fuselage of reference 1 is symmetrical about its midpoint.)

The blunt-tail cone of the present fuselage appears to increase the fuselage stability at high angles of attack.

Interference Increments

When the wing and fuselage are combined the effects of mutual interference on the contribution of each to the stability derivatives and the contribution of these components to the flow angularity at the tail are also to be considered. The mutual interference effects, ordinarily, are rather difficult to evaluate and are usually neglected except when test results are available for a model which closely resembles the airplane under consideration. In this event, recourse is made to a method (analogous to previous work, such as reference 7, for estimating the static lateral-stability derivatives of a complete model) which makes use of interference increments. These increments are designated Δ_1 and Δ_2 and the equation for estimating the derivative for a complete airplane is illustrated below in terms of C_{n_ψ}, for example:

$$C_{n_\psi} = C_{n_{\psi_F}} + C_{n_{\psi_W}} + \Delta_1 C_{n_\psi} + \Delta C_{n_{\psi_{V+H}}} + \Delta_2 C_{n_\psi}$$

The increment Δ_1 is the change in the derivative caused by mutual interference of the wing and fuselage for the model without the tail and can be obtained from test results in the manner illustrated by the following equation:

$$\Delta_1 C_{n_\psi} = C_{n_{\psi_{W+F}}} - \left(C_{n_{\psi_W}} + C_{n_{\psi_F}}\right)$$

This increment was determined for the test configurations and is shown in figures 9 and 10 for the static-stability and rolling-stability derivatives, respectively. The interference increment Δ_1 of both the static- and rolling-stability derivatives is generally small for the present tests except at angles of attack near the stall. For a high-wing or a low-wing configuration this increment would probably be somewhat larger even at small angles of attack.

The increment Δ_2 is directly concerned with the tail contribution and is the change in effectiveness of the tail caused by addition of the wing to the fuselage - tail-group configuration. The interference effects of the fuselage on the tail group are not determined. The increment Δ_2 is obtained from the test data as shown, for example, by the following equation for $\Delta_2 C_{n_\psi}$:

$$\Delta_2 C_{n_\psi} = \left(C_{n_{\psi_{W+F+V+H}}} - C_{n_{\psi_{W+F}}}\right) - \left(C_{n_{\psi_{F+V+H}}} - C_{n_{\psi_F}}\right)$$

This increment is combined with the estimated $\Delta C_{n_{\psi_{V+H}}}$ to give the total estimated tail contribution. It should be remembered, however, that the increment Δ_2 can be used to determine tail contributions for an airplane only when it is obtained from tests of a model which closely resembles the airplane under consideration. The increments Δ_2 of the static lateral-stability and rolling-stability derivatives of the test configurations are shown in figures 11 and 12, respectively. These figures show that the values of the increment Δ_2 of the static lateral-stability derivatives are very nearly zero for low and moderate angles of attack, whereas the increments of the rolling-stability derivatives are relatively large even at small angles of attack. Since the increment Δ_2 depends largely on the resultant of the sidewash caused by unsymmetrical span loading and the sidewash caused by vortices arising as a result of wing-fuselage interference, the magnitude of Δ_2 is an indication of the extent to which the derivatives are affected by the sidewash. Therefore, it can be concluded that, for the configurations considered, sidewash from the unsymmetrical wing loading due to sideslip and from the vortices arising from the wing-fuselage interference is of little importance except at high angles of attack. Large sidewash effects, however, are indicated on the rolling derivatives C_{Y_p} and C_{n_p} even at low angles of attack. These results indicated, therefore, that the equations currently used to calculate the various stability derivatives could be used for calculating the static-stability derivatives for configurations with wing on and with wing off without introducing an appreciable error, at least at small angles of attack, by neglecting sidewash effects from these sources. Some correction to the equations for computing the rolling derivatives appears necessary, however, to reduce the error that would be incurred by neglecting sidewash from the sources mentioned; therefore, the sidewash angles at the position of the vertical tail were measured in order to determine an approximate correction to the currently available equations. Furthermore, since it is expected that the wing-fuselage interference effects of the midwing configuration are small (as indicated in reference 8 for 0° angle of attack), the resultant sidewash (from the sources previously mentioned) can be attributed mainly to the unsymmetrical span loading on the wing during roll. Consequently, the increment of sidewash angle caused by wing alone, that is, by the unsymmetrical span loading of the wing during roll, was determined for several angles of attack at a value of l_V/b of 0.427 and for an angle of attack of 0° at a value of l_V/b of approximately 0.854.

The results of the measurements are shown in figure 13. The fact that the distributions below the center line of the tunnel are somewhat distorted because of the presence of the strut should be noted. The distributions above the tunnel center line (positive h/b) should be more reliable. For the measurements at $\frac{l_V}{b} = 0.427$ there appears to be only a small change in the sidewash distribution up to 12° angle of attack. The slight change of distribution at 12° angle of attack is to be expected since 12° is above the linear range of the lift curve, and some part of the wing may be stalled. Since the changes in distribution are small, the effective sidewash at the tail probably does not vary to a great extent with angle of attack in this range even though the position of the tail relative to these sidewash distributions changes with angle of attack of the model. Figure 13 shows little difference in the sidewash angle as the distance from the model mounting point is increased from $\frac{l_V}{b} = 0.427$ to $\frac{l_V}{b} = 0.855$.

Tail Contributions

On the basis of the foregoing discussion, the currently available equations for computing static lateral-stability derivatives, in terms of the estimated lift-curve slope of the tail, can be used for calculating both the wing-on and wing-off tail contributions with approximately equal accuracy. These equations are

$$\Delta C_{Y_\psi} = C_{L_{\alpha_V}} \frac{S_V}{S_W}$$

$$\Delta C_{n_\psi} = -C_{L_{\alpha_V}} \frac{S_V}{S_W b} \left(l_V \cos \alpha + z \sin \alpha \right)$$

$$\Delta C_{l_\psi} = -C_{L_{\alpha_V}} \frac{S_V}{S_W b} \left(l_V \sin \alpha - z \cos \alpha \right)$$

For the rolling derivatives, however, a correction to the previously used equations (as given in reference 9) is indicated to account for the sidewash caused by the unsymmetrical span loading on the wing during rolling. For rolling, therefore, the angle of attack in degrees at the vertical-tail center of pressure can be expressed as

$$\alpha_{V_z} = -57.3 \frac{pb}{2V} \left[\frac{2}{b} \left(z \cos \alpha - l_V \sin \alpha \right) - \frac{\partial \sigma}{\partial \frac{pb}{2V}} \right]$$

where the appropriate values of $\frac{\partial\sigma}{\partial\frac{pb}{2V}}$ should be the average effective sidewash parameter over the span of the vertical tail. Use of the equation for α_{V_z} leads to

$$\Delta C_{Y_p} = -57.3 C_{L_{\alpha_V}} \frac{S_V}{S_W}\left[\frac{2}{b}(z\cos\alpha - l_V\sin\alpha) - \frac{\partial\sigma}{\partial\frac{pb}{2V}}\right]$$

$$\Delta C_{n_p} = 57.3 C_{L_{\alpha_V}} \frac{S_V}{S_W}\left[\frac{1}{b}(z\sin\alpha + l_V\cos\alpha)\right]\left[\frac{2}{b}(z\cos\alpha - l_V\sin\alpha) - \frac{\partial\sigma}{\partial\frac{pb}{2V}}\right]$$

$$\Delta C_{l_p} = -57.3 C_{L_{\alpha_V}} \frac{S_V}{S_W}\left[\frac{1}{b}(z\cos\alpha - l_V\sin\alpha)\right]\left[\frac{2}{b}(z\cos\alpha - l_V\sin\alpha) - \frac{\partial\sigma}{\partial\frac{pb}{2V}}\right]$$

These equations apply only to the vertical tail. An additional contribution to C_{l_p} is due to the damping in roll of the horizontal tail. This contribution, however, is small and should be approximately independent of angle of attack.

Although the exact effective value of the sidewash parameter is not easily determined, an approximate value can be obtained from the sidewash plots. As was mentioned before, the angle-of-attack effect on the sidewash parameter through 12° angle of attack is not very large and, since knowledge of the tail contributions is probably most important for this range, an average value of $\frac{\partial\sigma}{\partial\frac{pb}{2V}}$ of 0.25 was obtained from the plots and is considered to be a fairly good approximation for the entire angle-of-attack range of the arrangement tested. For the wing-off condition $\frac{\partial\sigma}{\partial\frac{pb}{2V}}$ is of course assumed to be zero.

In order to show the experimental tail contributions and the accuracy with which they can be predicted by calculations, figures 14 and 15 were prepared. In figure 14 are presented the test values of the

increments of C_{Y_ψ}, C_{n_ψ}, and C_{l_ψ} contributed by the vertical tail with and without the horizontal tail and with wing on and off. In figure 15 are presented the increments of rolling-stability derivatives contributed by the tail for the three tail configurations with wing on and wing off, together with those calculated by the previously listed equations. These figures also show the values of the derivatives calculated by the equations based on estimated values of $C_{L_{\alpha_V}}$. The value of $C_{L_{\alpha_V}}$ used for each tail configuration was obtained from reference 3 after the effective aspect ratio for the particular configuration was estimated by the methods of reference 10. No aspect-ratio correction was made for the case of no horizontal tail; however, the large discrepancy between the measured and calculated values of the increments of C_{Y_ψ} and C_{n_ψ} indicates that a large end-plate effect is contributed by the blunt tail cone. The fact that the values calculated for the configuration with the low horizontal tail on (fig. 14(b)) would be in good agreement almost up to the angle of maximum lift with the test results for the other tail configurations (figs. 14(a) and 14(c)) indicates that the end-plate effect of the fuselage is roughly equivalent to that of the horizontal tail in the low position. Some quantitative information on this effect is given in reference 11.

As was expected on the basis of the small values of the increment Δ_2 of the static-stability derivatives (fig. 11), there are only small differences in the tail contributions for the wing-on and wing-off tail configurations almost to the angle of maximum lift (fig. 14). At higher angles of attack the discrepancy between wing-on and wing-off results was greater and larger sidewash effects were thus indicated.

From figure 15 it can be seen that the calculations predict the wing-off values of the rolling-stability derivatives at low angles of attack with reasonable accuracy except perhaps ΔC_{n_p} for the case with the horizontal tail in the low position. A value of ΔC_{n_p} of 0.036, which was calculated for 0° angle of attack by using the measured value of ΔC_{Y_p}, indicates that there is a forward shift of the center of pressure of the vertical tail caused by the horizontal tail. This forward shift accounts for an appreciable part of the difference between the calculated and measured values.

The large discrepancy between the calculated and measured wing-off values of the rolling derivatives ΔC_{Y_p} and ΔC_{n_p} at the high angles of attack probably is caused by sidewash as a result of the development of lateral forces on the fuselage during roll. This result indicates that either measurements of the sidewash caused by the fuselage or a means of

estimating this sidewash is necessary if better accuracy in predicting ΔC_{Y_p} and ΔC_{n_p} is expected at higher angles of attack. Part of this discrepancy at higher angles of attack probably can be attributed to the fact that the equations for the rolling derivatives are based on the assumption that, during roll, the entire tail is operating at the angle of attack which occurs at the center of pressure of the tail. For the actual case, however, the angle of attack at any section of the tail depends on the distance of that section from the axis of rotation of the model.

According to the methods used up to the present time, the curves calculated for the wing-off values of the derivatives would also be used to predict the wing-on values. This procedure would lead to an appreciable error especially when estimates are made of the tail contribution to C_{Y_p} and C_{n_p} at small and medium angles of attack. The accuracy of predicting the tail contribution to C_{l_p} would not be affected to a great extent. The contribution of the tail configuration tested to the damping in roll is small because of the short distance from the vertical-tail center of pressure to the axis of roll, and this contribution is little-affected by load changes caused by the wing. Figure 15 indicates that a much more accurate estimate of the wing-on values of ΔC_{Y_p} and ΔC_{n_p} is obtained by using the equations which approximately account for the wing sidewash effect than is obtained by the methods used in the past (wing off), which neglect sidewash. Generally, the wing-on values are predicted with good accuracy for angles of attack near zero and, as was mentioned, if the sidewash effects caused by the fuselage (wing off) could be accounted for, a more accurate estimate could probably be obtained at the higher angles of attack.

The equations, in which measured values of ΔC_{Y_ψ} rather than $C_{L_\alpha} \frac{S_V}{S_W}$ are used for estimating the tail contributions to the rolling derivatives, were also rewritten to include the sidewash parameter and are

$$\Delta C_{Y_p} = -57.3 \Delta C_{Y_\psi} \left[\frac{2}{b} (z \cos \alpha - l_V \sin \alpha) - \frac{\partial \sigma}{\partial \frac{pb}{2V}} \right]$$

$$\Delta C_{n_p} = 57.3\Delta C_{Y_\psi}\left[\frac{l}{b}(z \sin \alpha + l_V \cos \alpha)\right]\left[\frac{2}{b}(z \cos \alpha - l_V \sin \alpha) - \frac{\partial\sigma}{\partial\frac{pb}{2V}}\right]$$

$$\Delta C_{l_p} = -57.3\Delta C_{Y_\psi}\left[\frac{l}{b}(z \cos \alpha - l_V \sin \alpha)\right]\left[\frac{2}{b}(z \cos \alpha - l_V \sin \alpha) - \frac{\partial\sigma}{\partial\frac{pb}{2V}}\right]$$

These equations are particularly useful for estimating the tail contributions for any tail configuration for which an accurate estimate of the lift-curve slope cannot be made and measured values of ΔC_{Y_ψ} for an appropriate model are available. In figure 16 are compared the values of the rolling derivatives calculated by the use of these equations with the measured results. Generally, the calculated results (wing on and wing off) are of about the same accuracy as those calculated by the use of the equations based on estimated lift-curve slope.

The results discussed are for a midwing configuration and the conclusions, especially those relating to wing-fuselage interference effects, might be considerably altered for a high-wing or low-wing configuration.

CONCLUSIONS

The results of an investigation to determine the effect of an unswept wing on the contribution of unswept-tail configurations to the low-speed static- and rolling-stability derivatives of a midwing model indicate the following conclusions:

1. At angles of attack almost to the angle of maximum lift, there are only small differences in the tail contributions to the static lateral-stability derivatives with wing on or wing off. For this range of angles of attack the contribution of the tail can be estimated fairly accurately by the available procedures.

2. The available procedures generally predict the wing-off values of the rolling derivatives at low angles of attack with reasonable accuracy. Altering these equations to account for sidewash caused by the unsymmetrical wing loading (due to roll) brings the calculated wing-on values into much better agreement with the measured wing-on values.

3. Some error in the estimated contribution of the tail to the yawing moment caused by roll results for the low-horizontal-tail

configuration because of a forward shift in the center of pressure of the vertical tail caused by the horizontal tail.

4. The contribution of the tail configuration tested to the damping in roll is small because of the short distance from the vertical-tail center of pressure to the axis of roll, and this contribution is little affected by load changes caused by the wing.

Langley Aeronautical Laboratory
National Advisory Committee for Aeronautics
Langley Air Force Base, Va., June 16, 1950

REFERENCES

1. Brewer, Jack D., and Lichtenstein, Jacob H.: Effect of Horizontal Tail on Low-Speed Static Lateral Stability Characteristics of a Model Having 45° Sweptback Wing and Tail Surfaces. NACA TN 2010, 1950.

2. MacLachlan, Robert, and Letko, William: Correlation of Two Experimental Methods of Determining the Rolling Characteristics of Unswept Wings. NACA TN 1309, 1947.

3. DeYoung, John: Theoretical Additional Span Loading Characteristics of Wings with Arbitrary Sweep, Aspect Ratio, and Taper Ratio. NACA TN 1491, 1947.

4. Toll, Thomas A., and Queijo, M. J.: Approximate Relations and Charts for Low-Speed Stability Derivatives of Swept Wings. NACA TN 1581, 1948.

5. Goodman, Alex, and Fisher, Lewis R.: Investigation at Low Speeds of the Effect of Aspect Ratio and Sweep on Rolling Stability Derivatives of Untapered Wings. NACA Rep. 968, 1950.

6. Goodman, Alex, and Adair, Glenn H.: Estimation of the Damping in Roll of Wings through the Normal Flight Range of Lift Coefficient. NACA TN 1924, 1949.

7. Recant, Isidore G., and Wallace, Arthur R.: Wind-Tunnel Investigation of Effect of Yaw on Lateral-Stability Characteristics. III - Symmetrically Tapered Wing at Various Positions on Circular Fuselage with and without a Vertical Tail. NACA TN 825, 1941.

8. Recant, Isidore G., and Wallace, Arthur R.: Wind-Tunnel Investigation of the Effect of Vertical Position of the Wing on the Side Flow in the Region of the Vertical Tail. NACA TN 804, 1941.

9. Bamber, Millard J.: Effect of Some Present-Day Airplane Design Trends on Requirements for Lateral Stability. NACA TN 814, 1941.

10. Murray, Harry E.: Wind-Tunnel Investigation of End-Plate Effects of Horizontal Tails on a Vertical Tail Compared with Available Theory. NACA TN 1050, 1946.

11. Queijo, M. J., and Wolhart, Walter D.: Experimental Investigation of the Effect of Vertical-Tail Size and Length and of Fuselage Shape and Length on the Static Lateral Stability Characteristics of a Model with 45° Sweptback Wing and Tail Surfaces. NACA TN 2168, 1950.

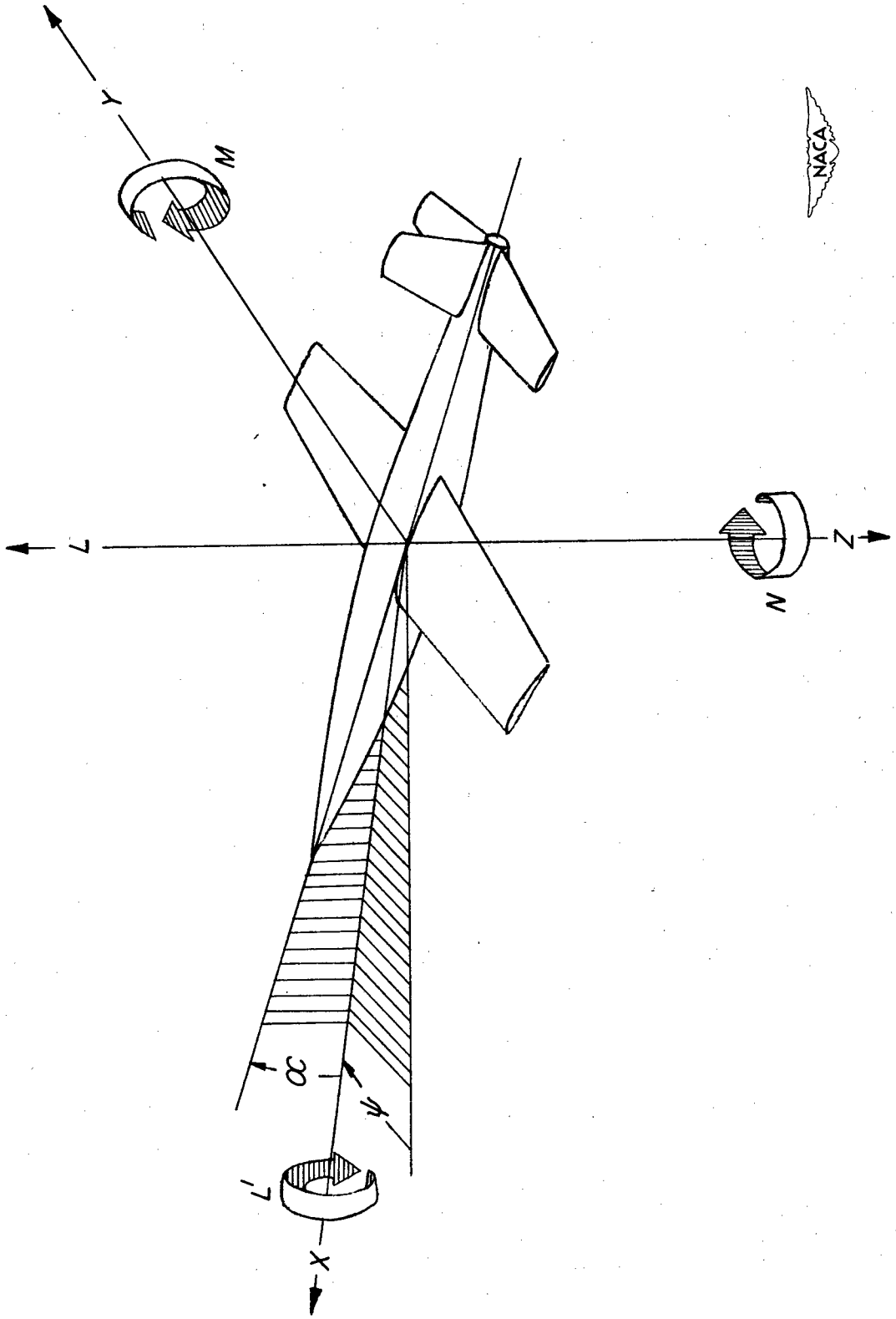

Figure 1.- System of axes used. Arrows indicate positive direction of angles, forces, and moments.

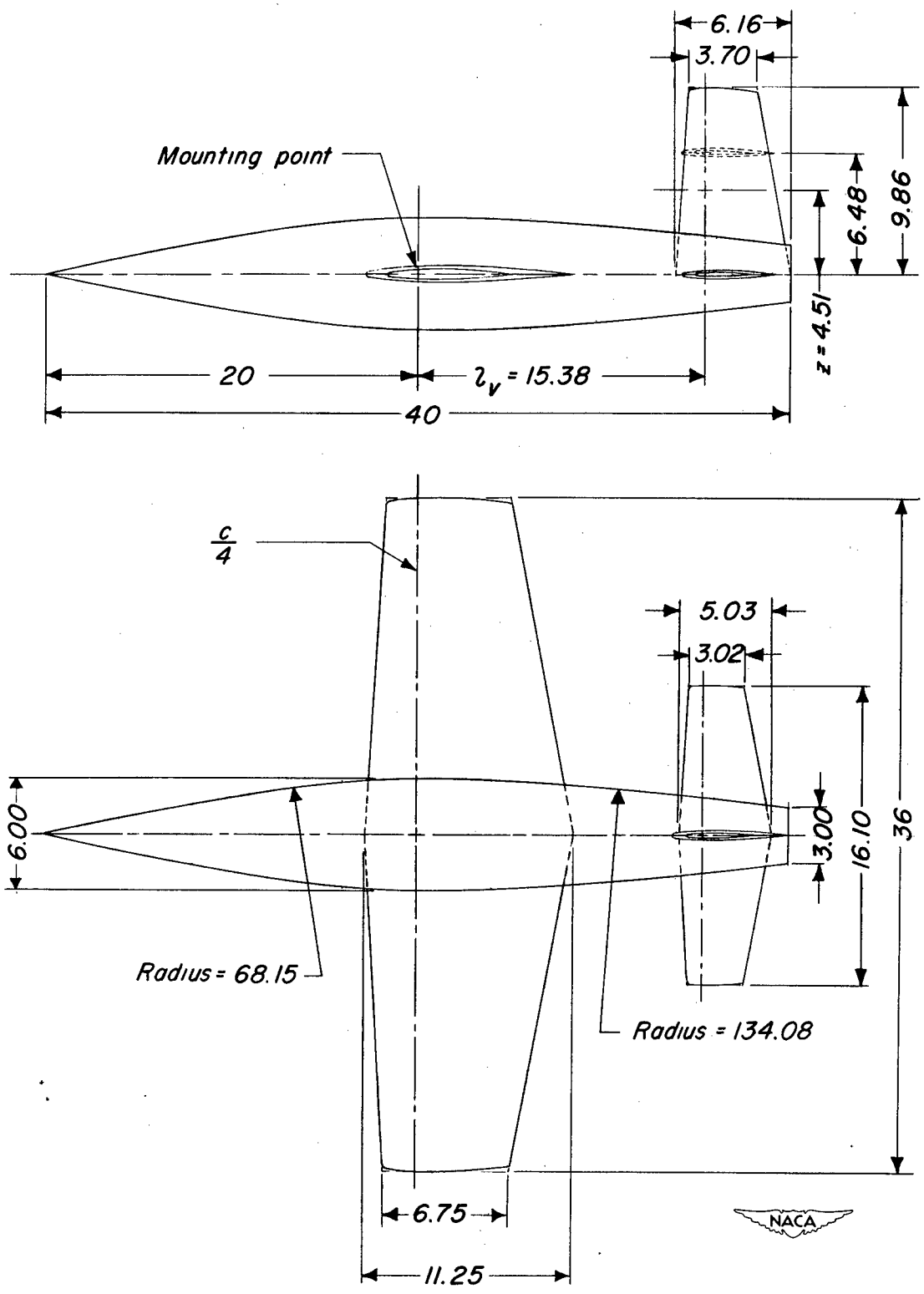

Figure 2.- Dimensions of the complete model. (All dimensions are in inches.)

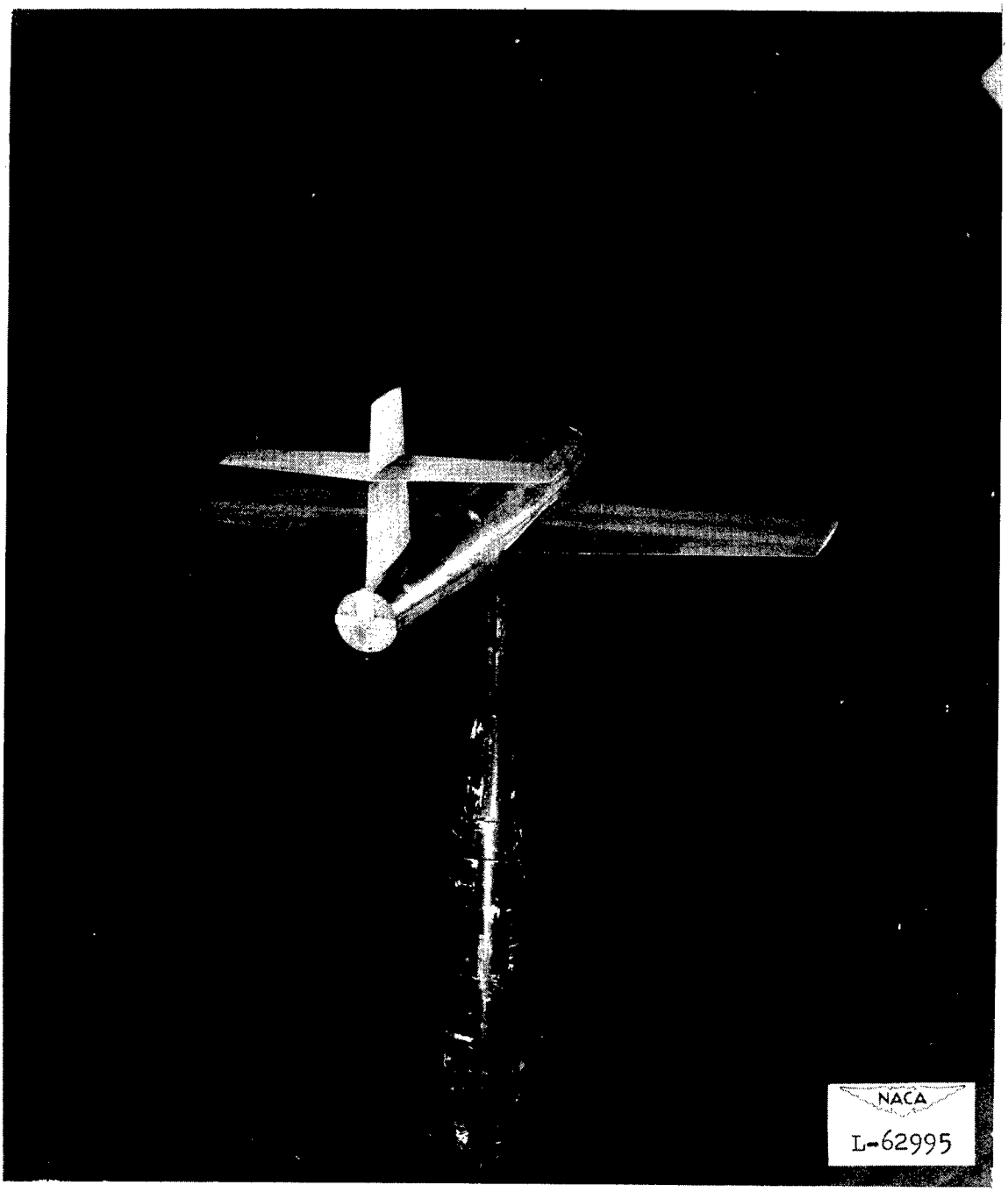

Figure 3.- Model with high horizontal tail mounted in the rolling-flow section of the Langley stability tunnel.

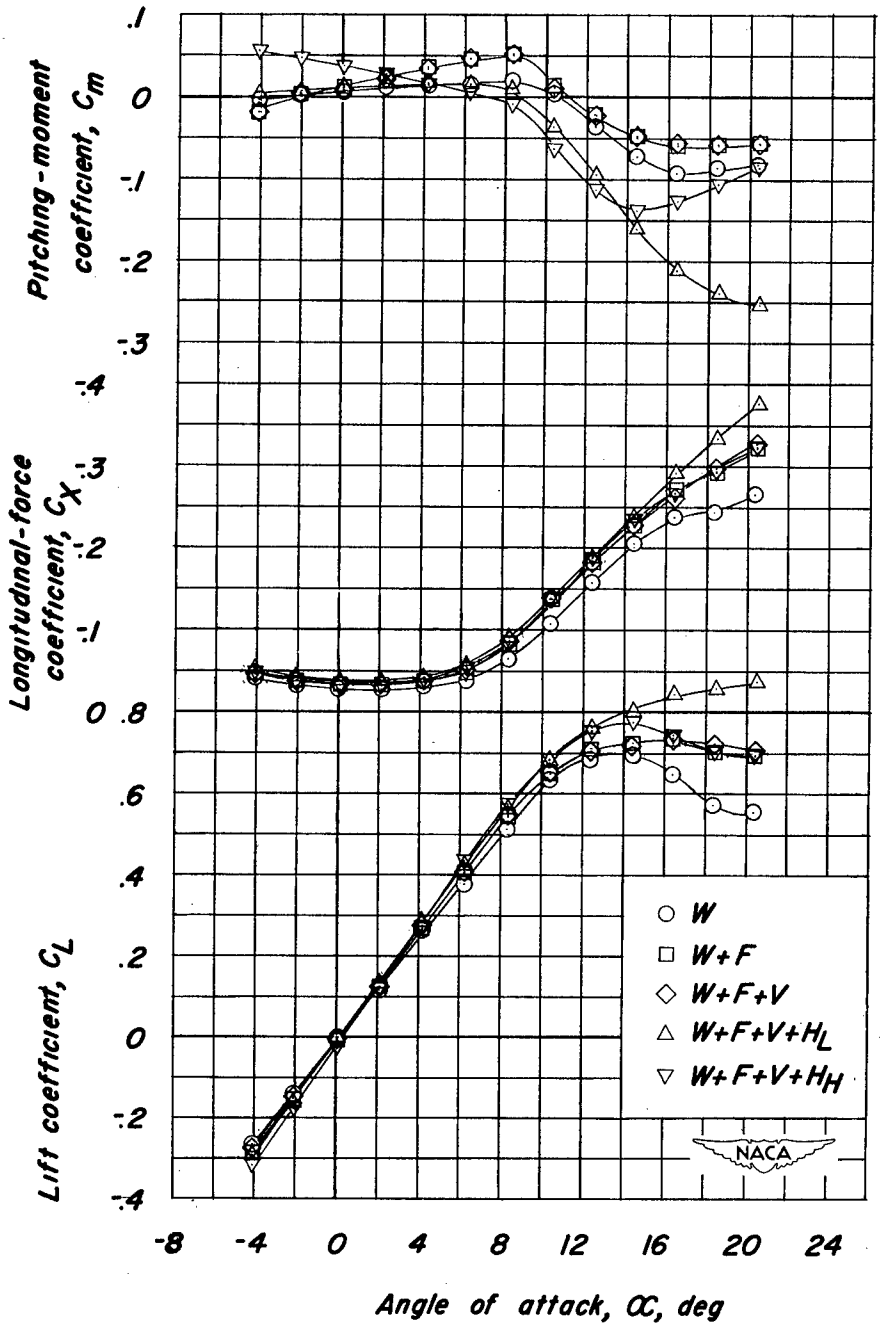

(a) Wing on.

Figure 4.- Aerodynamic characteristics of the basic configurations.

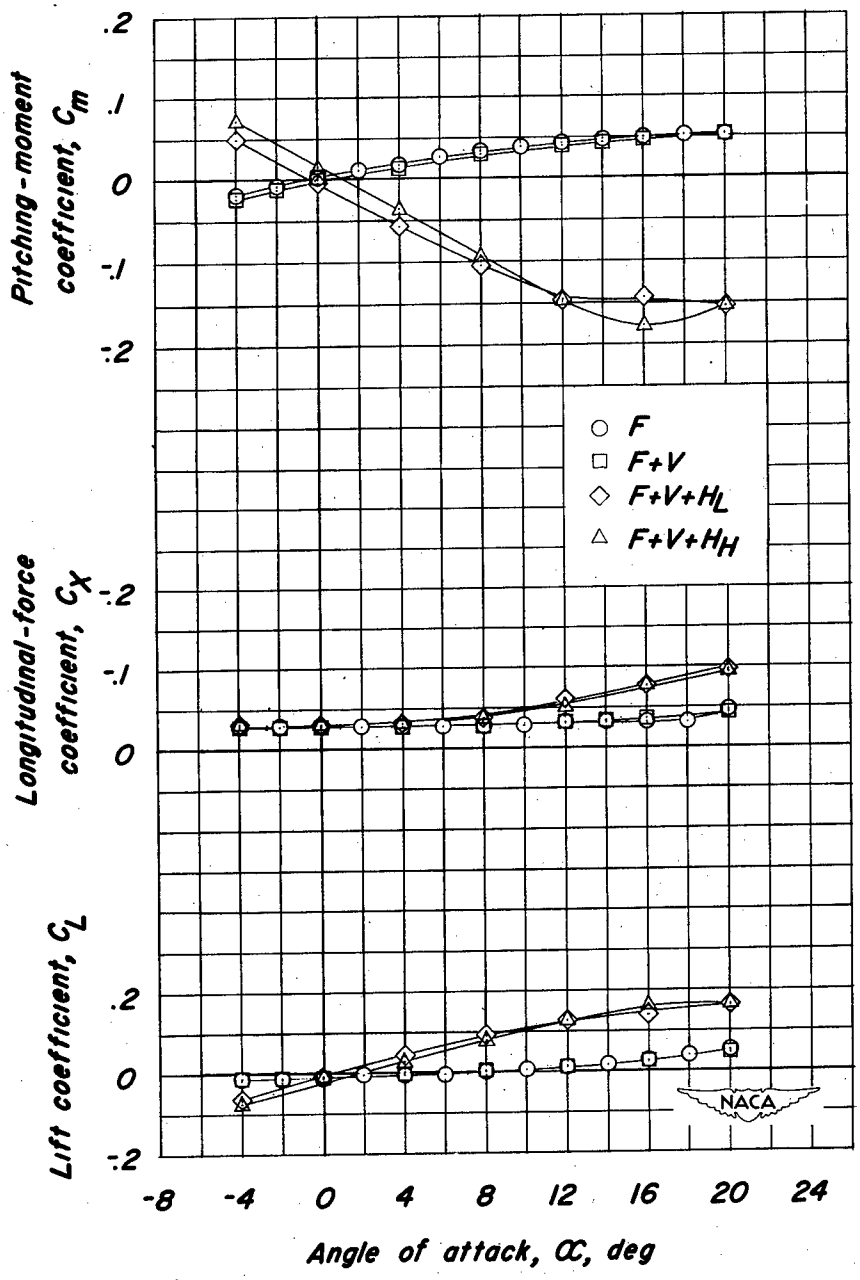

(b) Wing off.

Figure 4.- Concluded.

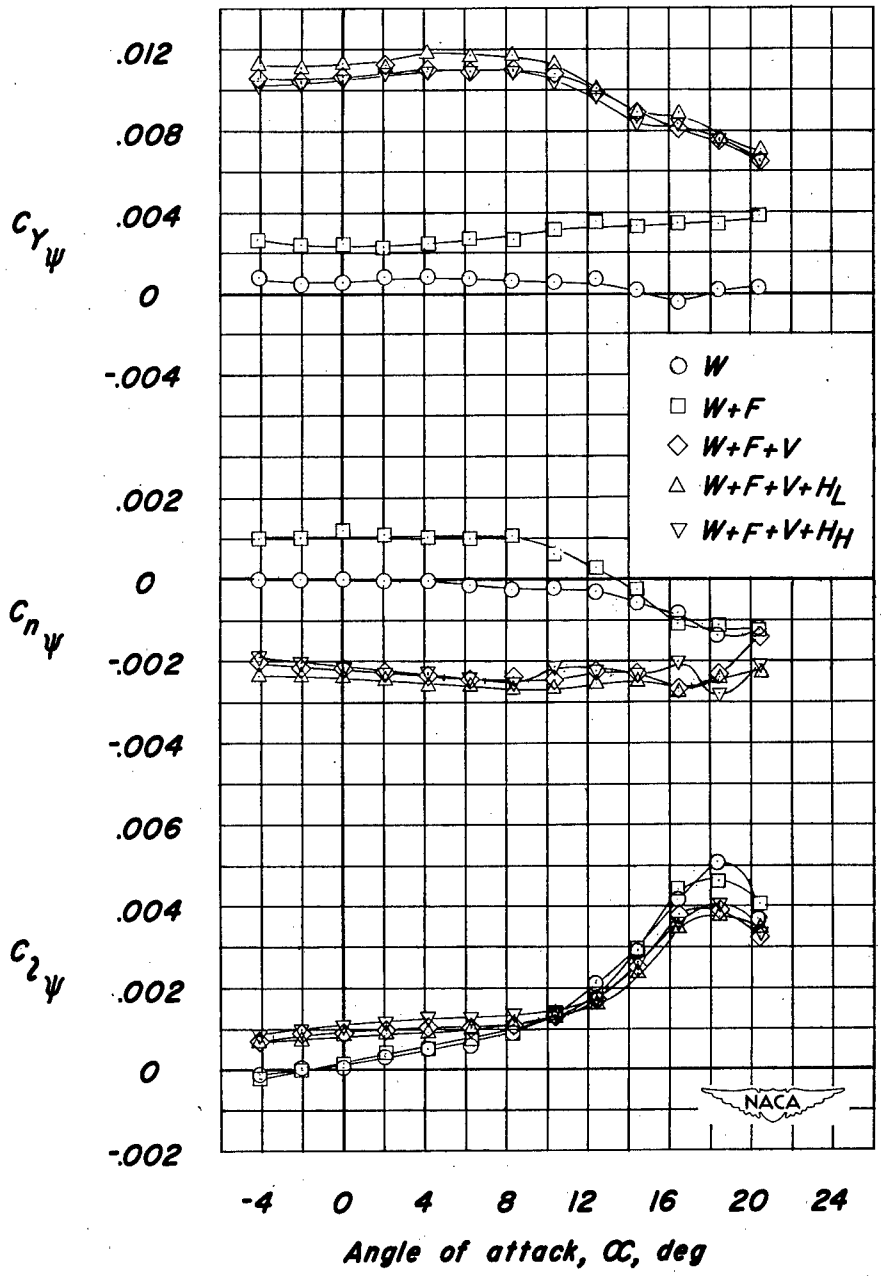

(a) Wing on.

Figure 5.- Variation with angle of attack of C_{Y_ψ}, C_{n_ψ}, and C_{l_ψ} of the basic configurations.

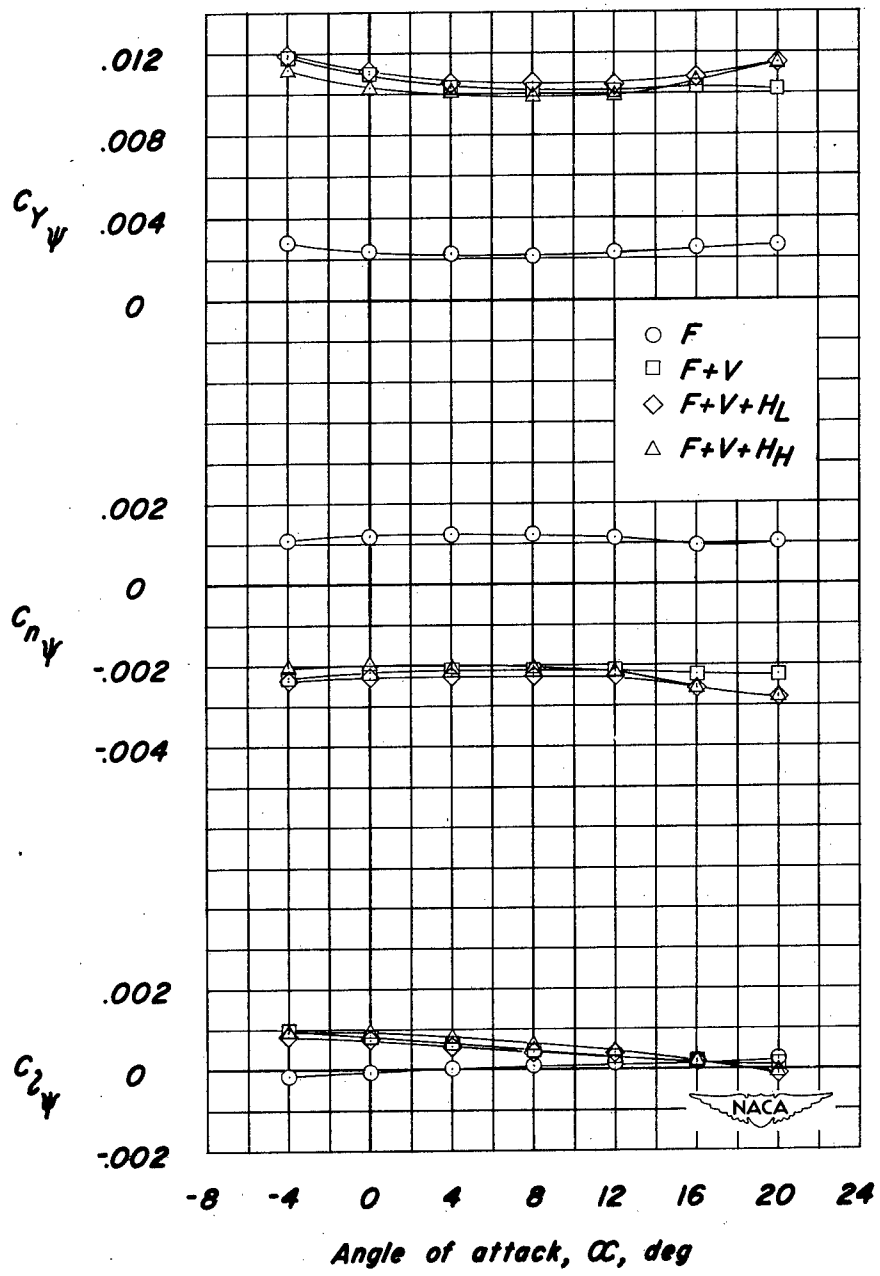

(b) Wing off.

Figure 5.- Concluded.

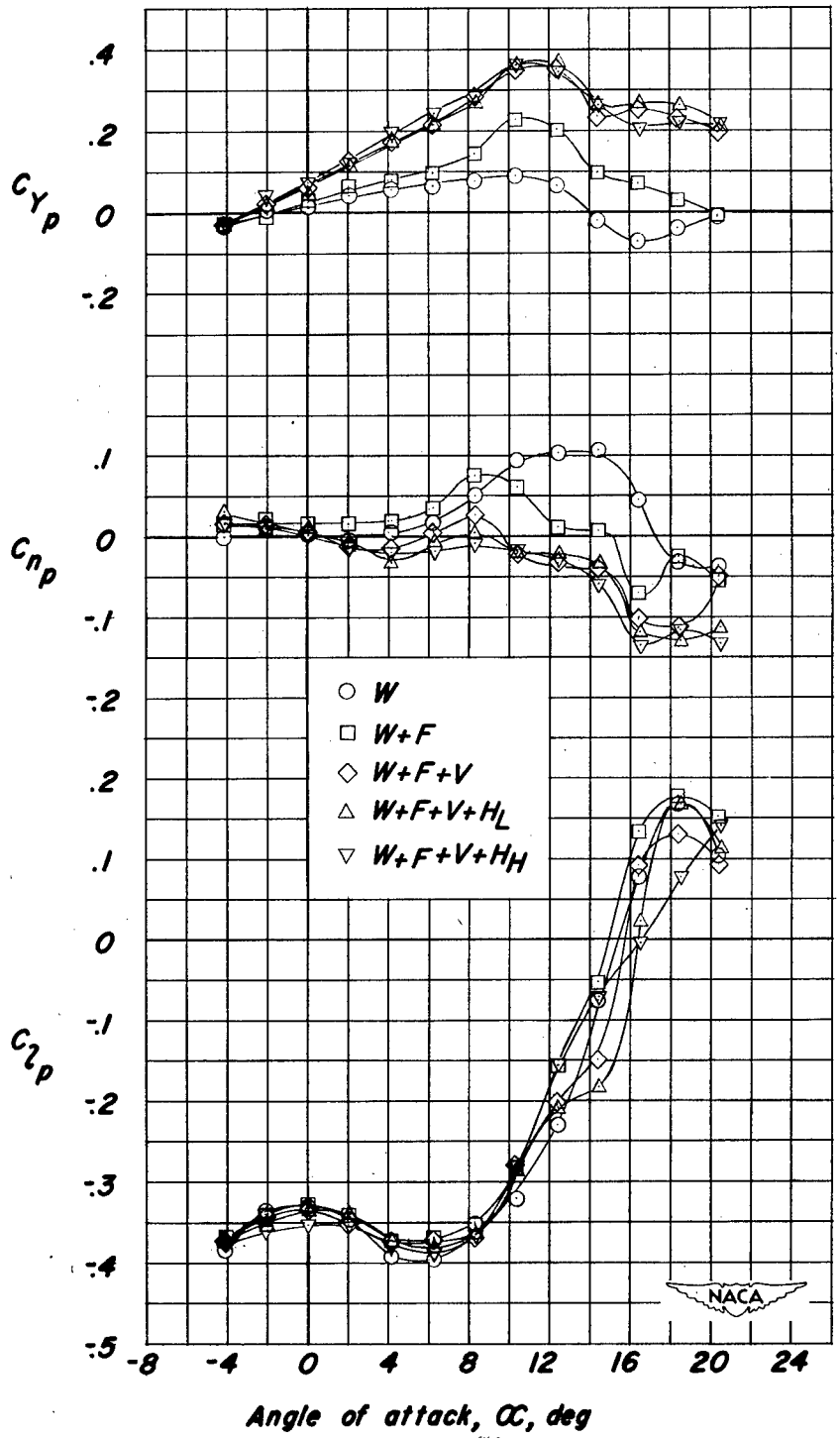

(a) Wing on.

Figure 6.- Variation with angle of attack of C_{Y_p}, C_{n_p}, and C_{l_p} of the basic configurations.

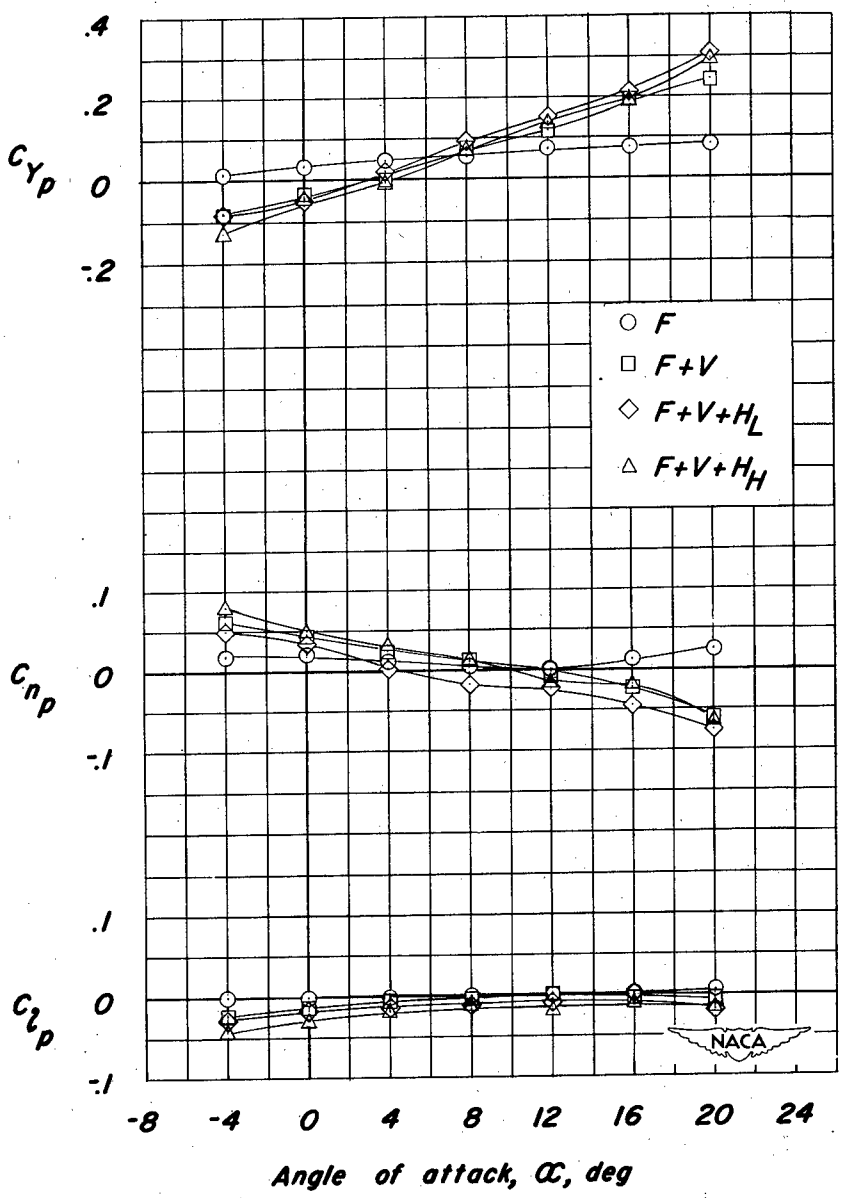

(b) Wing off.

Figure 6.- Concluded.

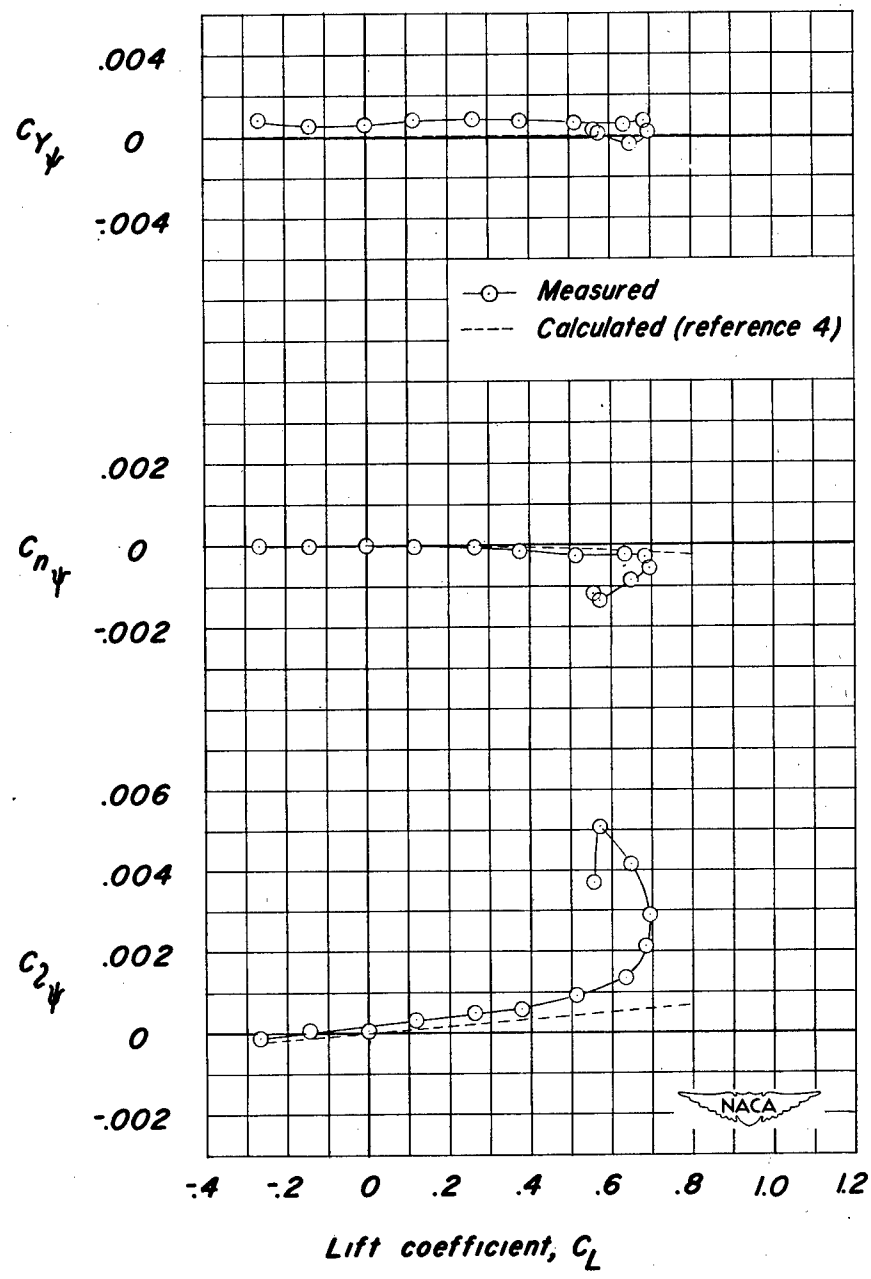

Figure 7.- Variation with lift coefficient of C_{Y_ψ}, C_{n_ψ}, and C_{l_ψ} for wing alone.

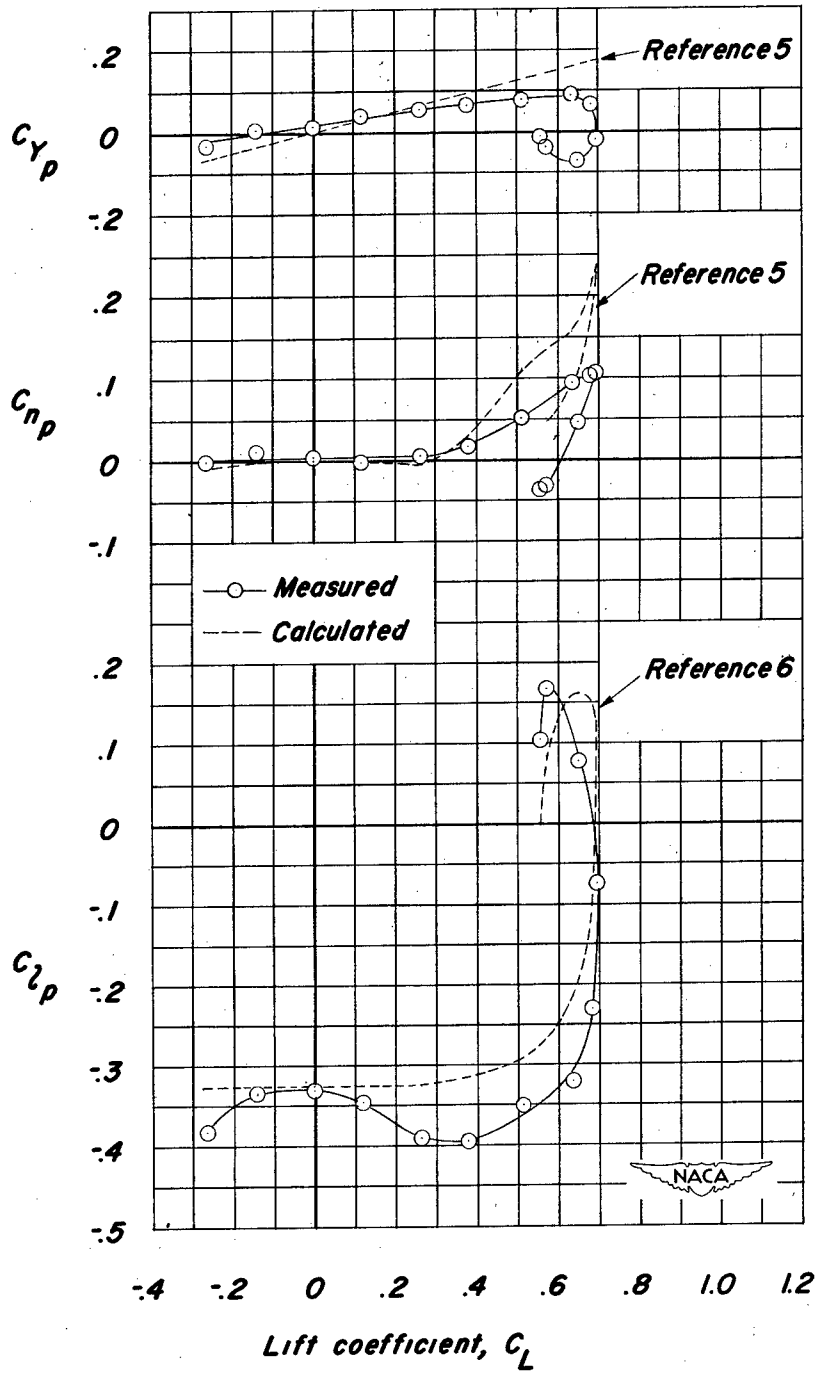

Figure 8.- Variation with lift coefficient of C_{Y_p}, C_{n_p}, and C_{l_p} for wing alone.

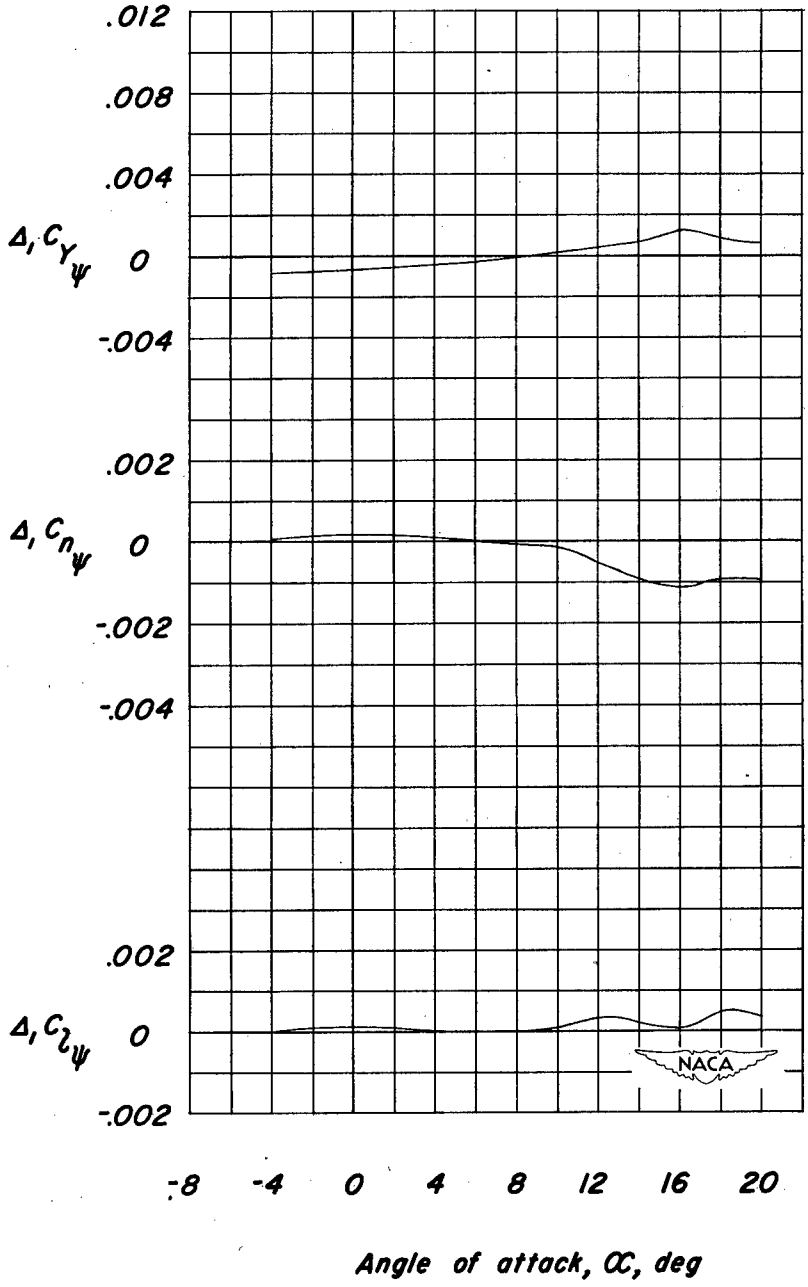

Figure 9.- Variation with angle of attack of the interference increments Δ_1 of C_{Y_ψ}, C_{n_ψ}, and C_{l_ψ}.

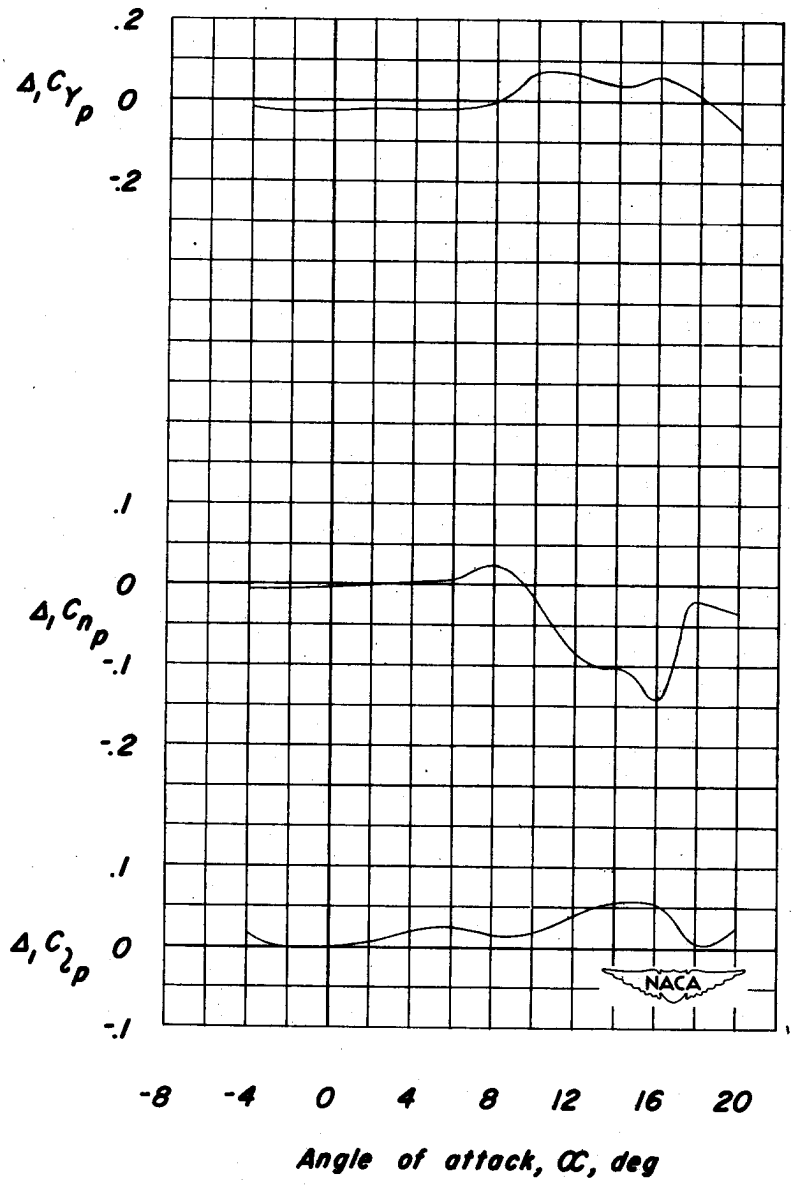

Figure 10.- Variation with angle of attack of the interference increments Δ_1 of C_{Y_p}, C_{n_p}, and C_{l_p}.

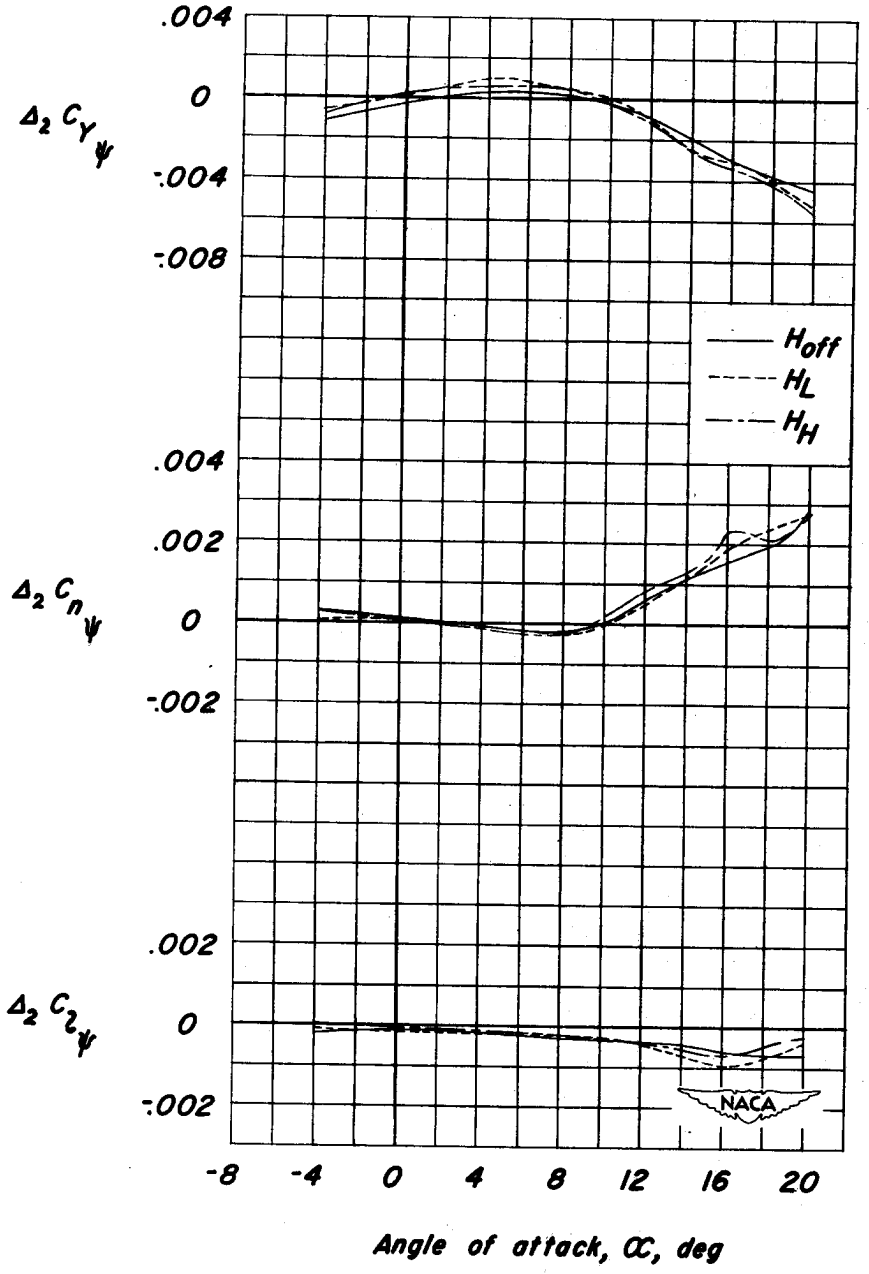

Figure 11.- Variation with angle of attack of the interference increments Δ_2 of C_{Y_ψ}, C_{n_ψ}, and C_{l_ψ}.

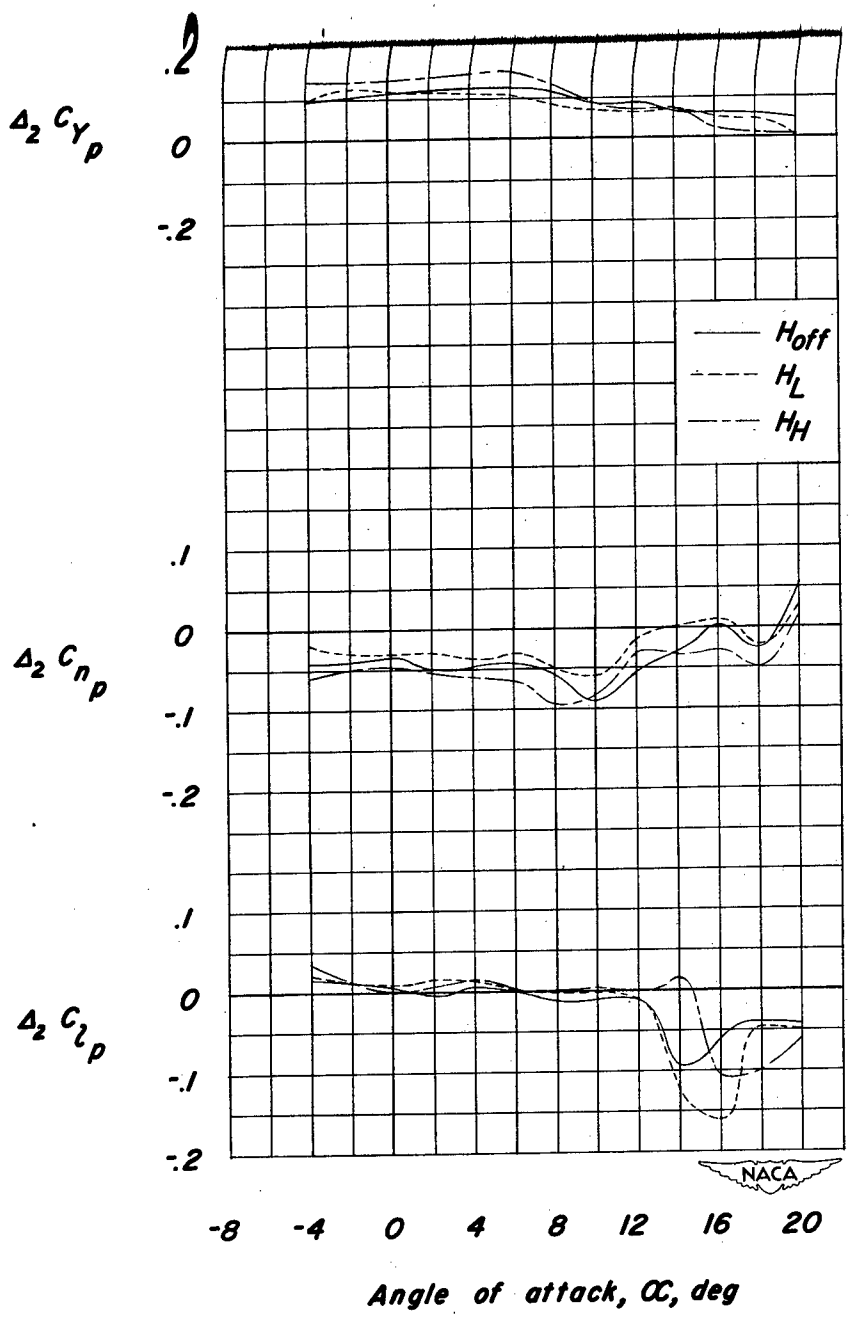

Figure 12.- Variation with angle of attack of the interference increments Δ_2 of C_{Y_p}, C_{n_p}, and C_{l_p}.

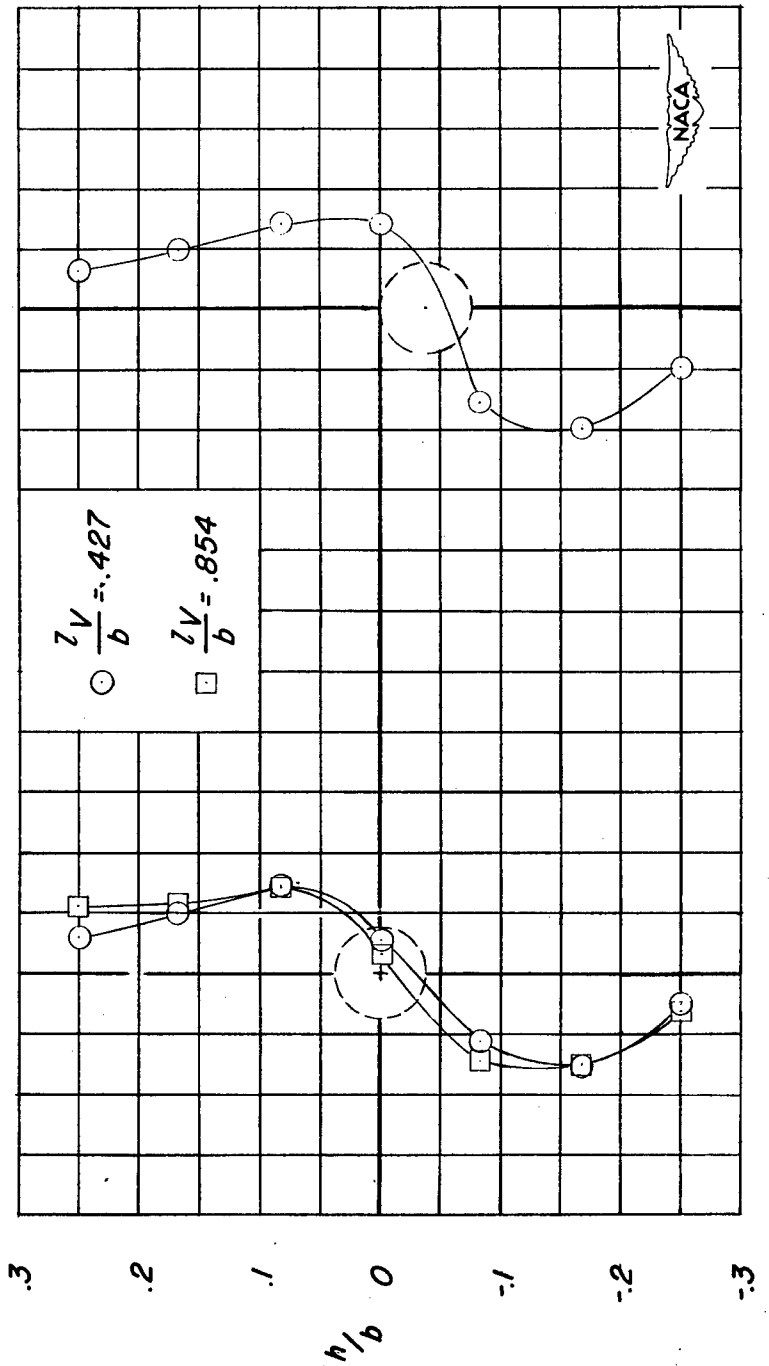

(a) $\alpha = 0.04°$. (b) $\alpha = 4.03°$.

Figure 13.- Variation of $\frac{\partial\sigma}{\partial\frac{pb}{2V}}$ with distance above and below the tunnel center line.

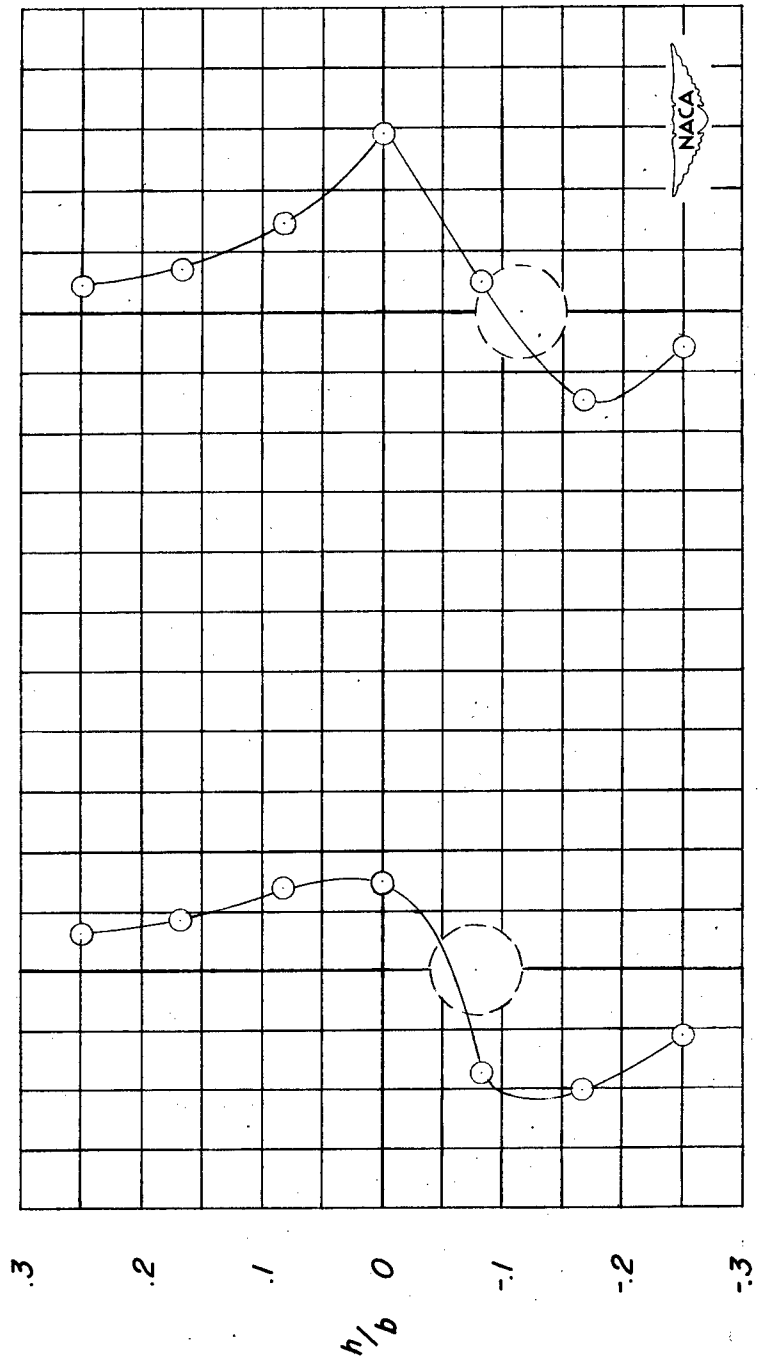

(c) $\alpha = 8.06°$.

(d) $\alpha = 12.1°$.

Figure 13.- Concluded.

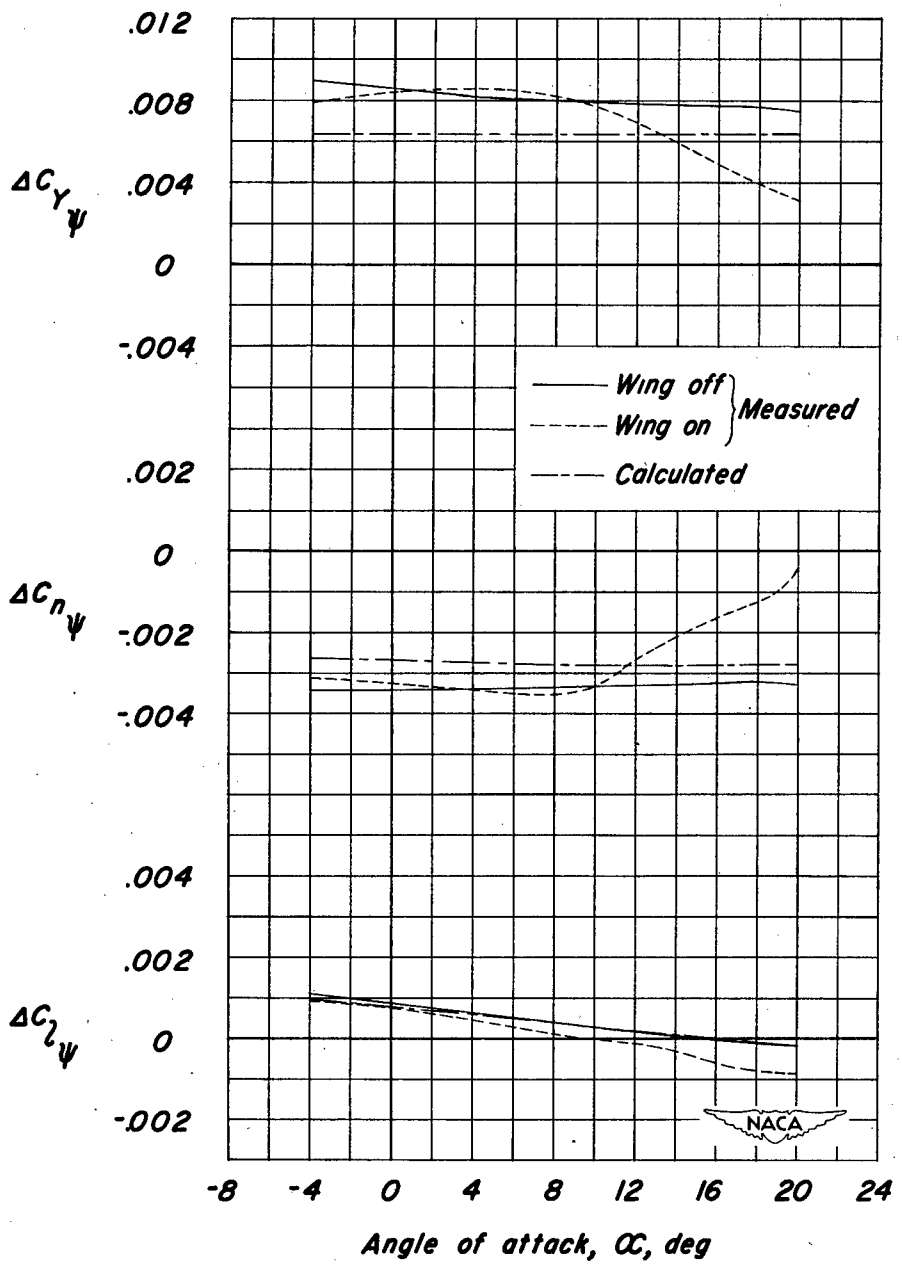

(a) Horizontal tail off.

Figure 14.- Comparison of the measured and calculated variation with angle of attack of the tail contributions ΔC_{Y_ψ}, ΔC_{n_ψ}, and ΔC_{l_ψ} for the model with wing on and wing off. Calculations based on estimated $C_{L_{\alpha_V}}$.

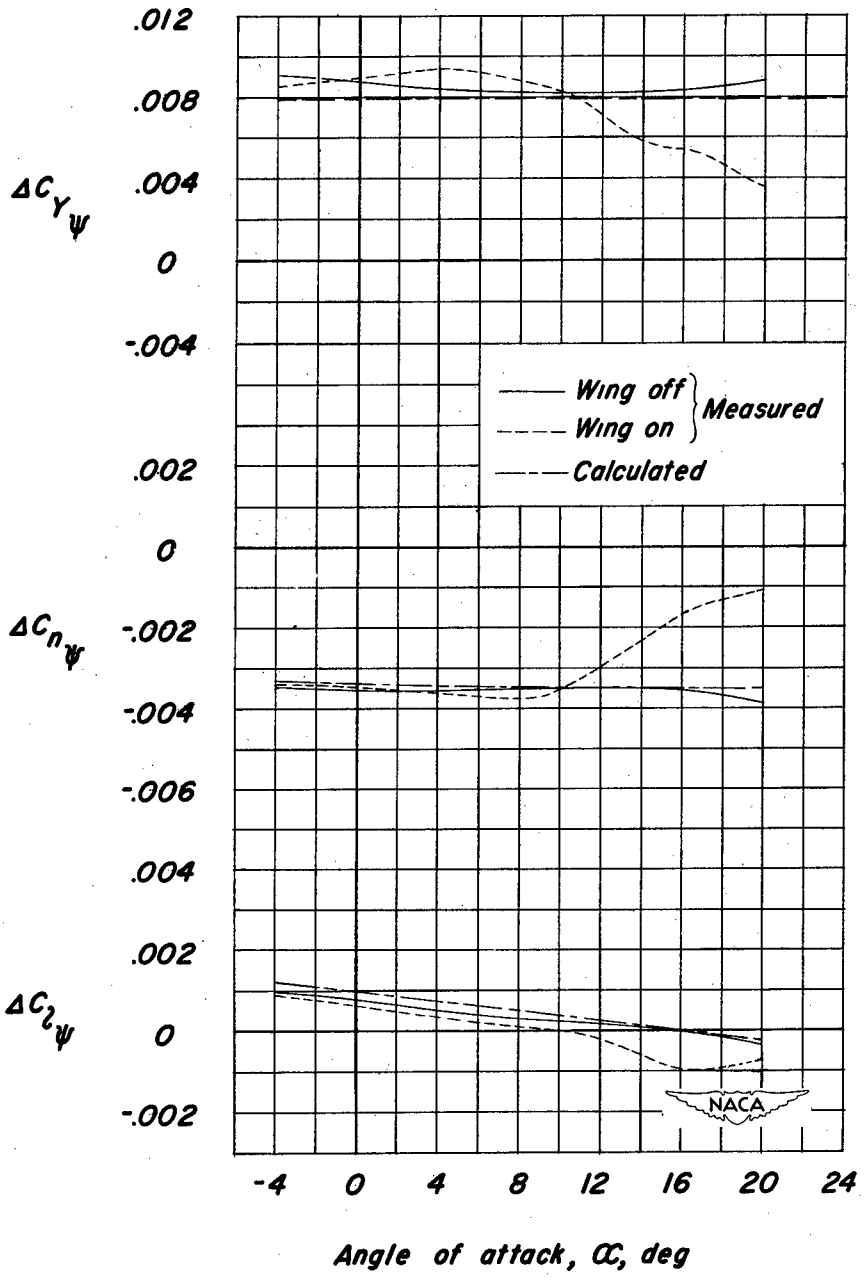

(b) Low horizontal tail.

Figure 14.- Continued.

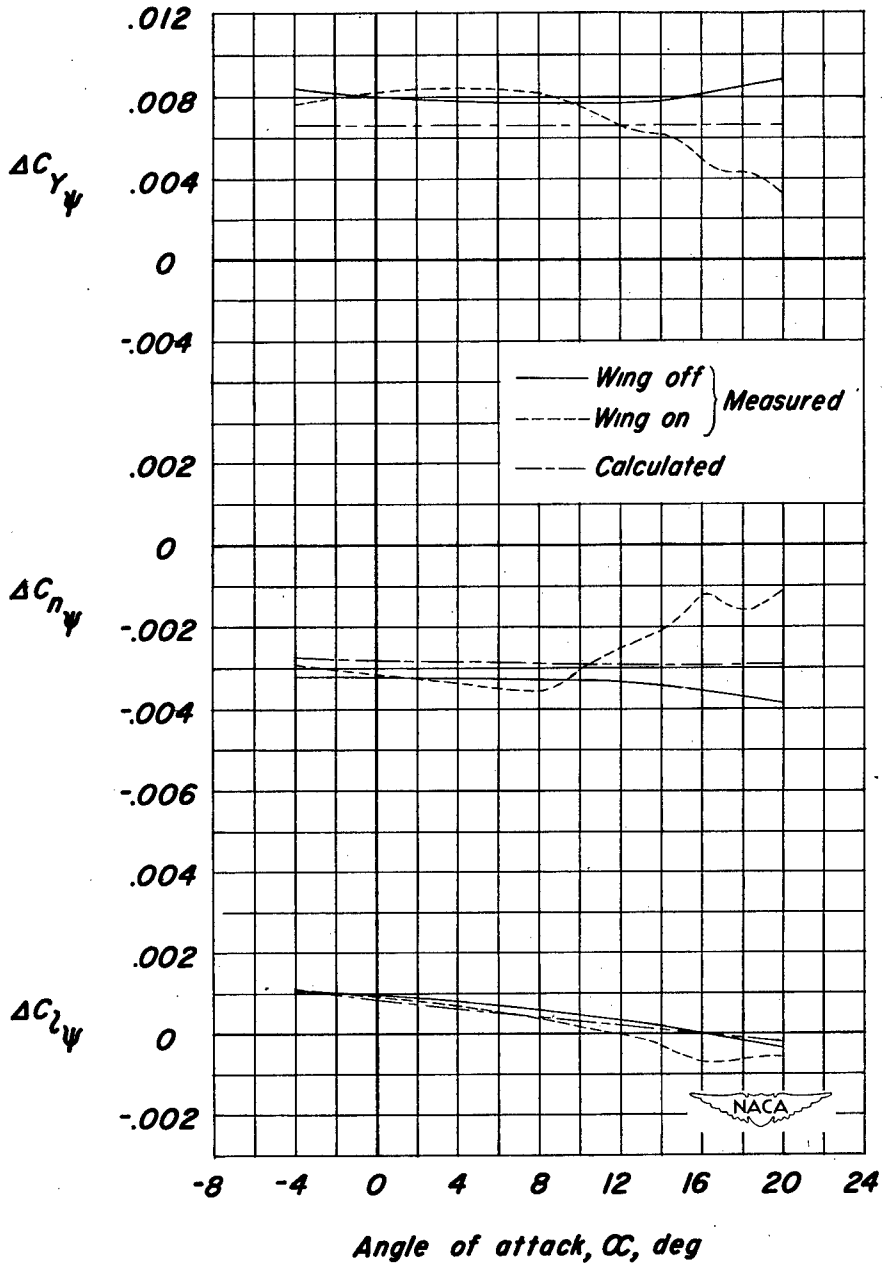

(c) High horizontal tail.

Figure 14.- Concluded.

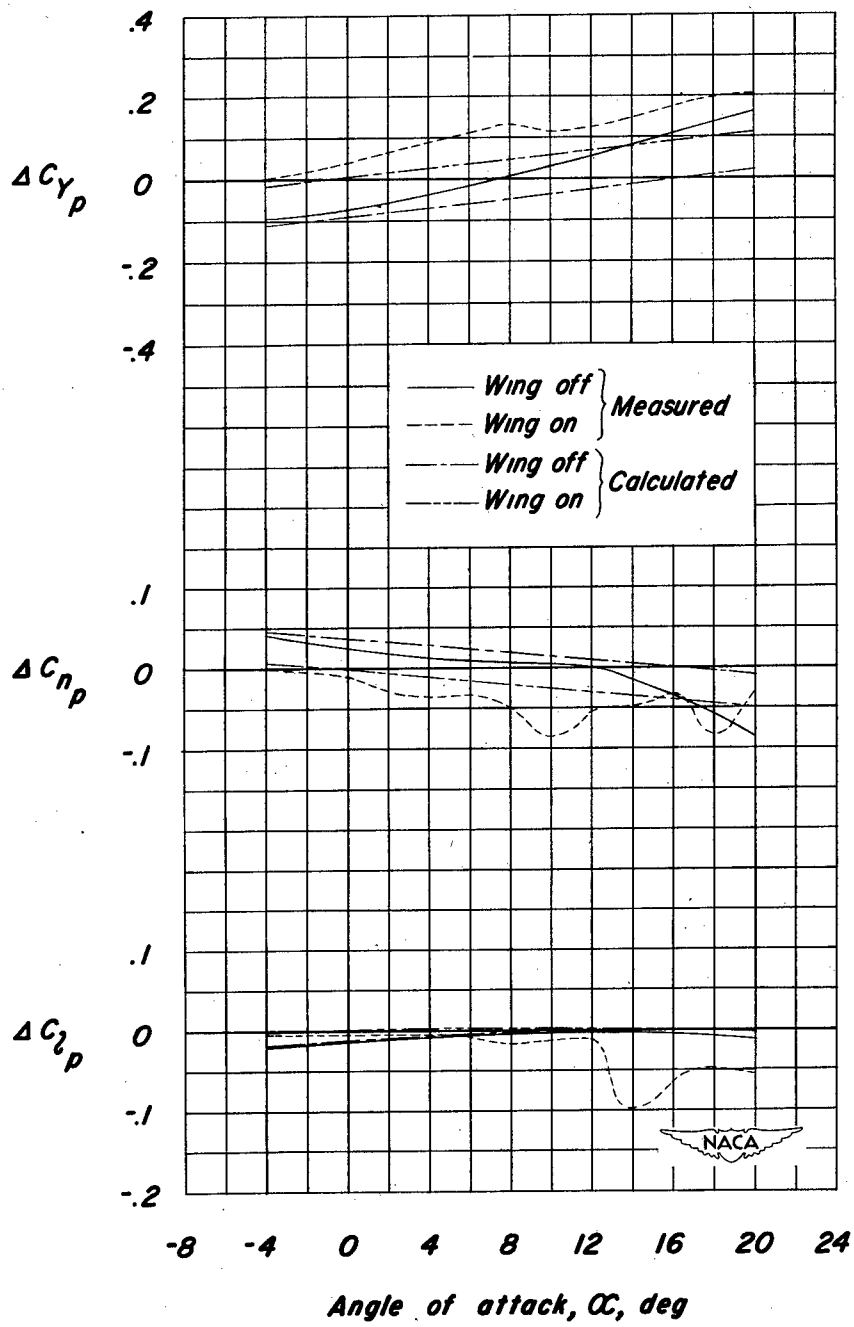

(a) Horizontal tail off.

Figure 15.- Comparison of the measured and calculated variation with angle of attack of the tail contributions ΔC_{Y_p}, ΔC_{n_p}, and ΔC_{l_p} for the model with wing on and wing off. Calculations based on estimated $C_{L_{\alpha_V}}$.

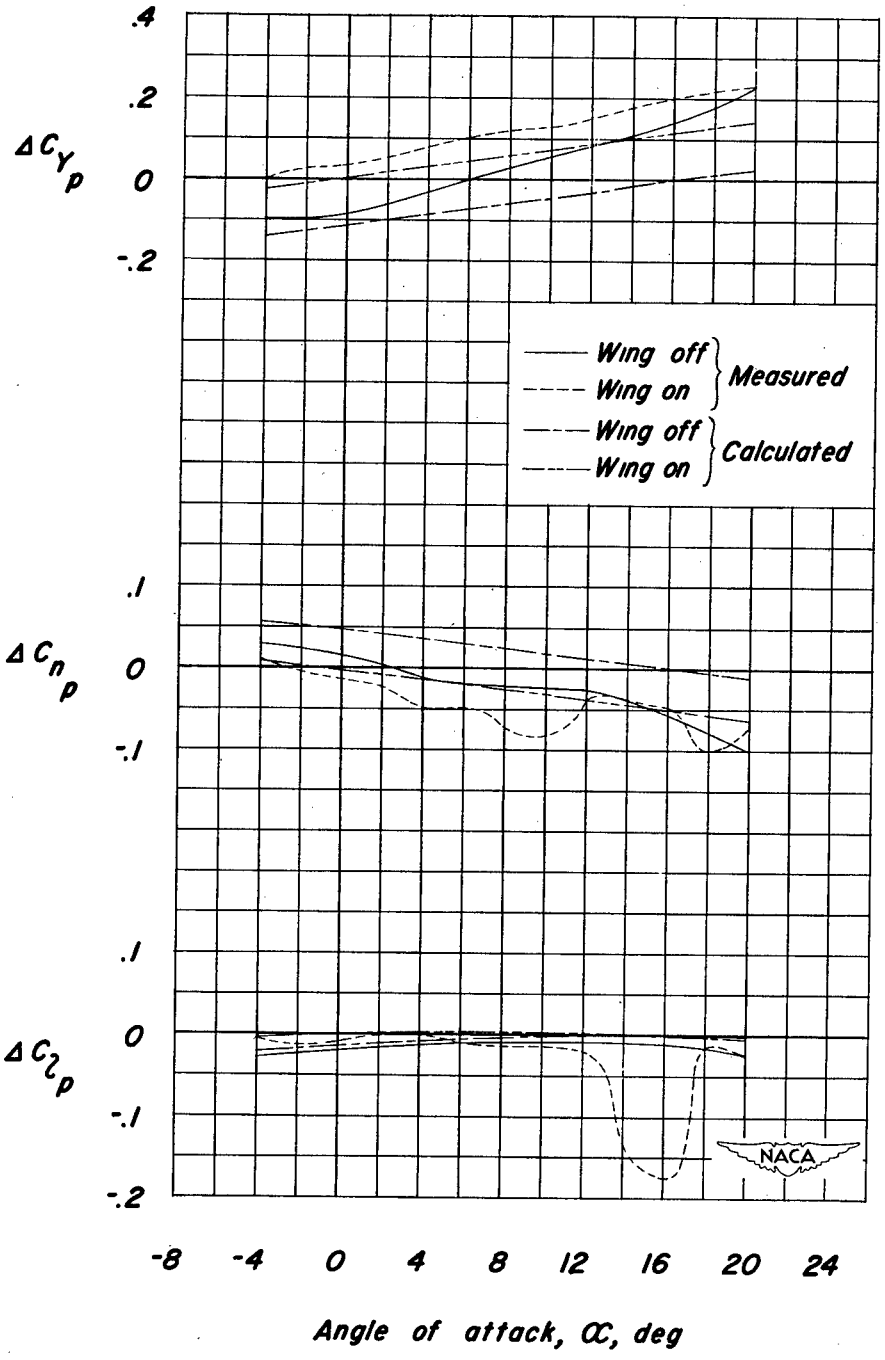

(b) Low horizontal tail.

Figure 15.- Continued.

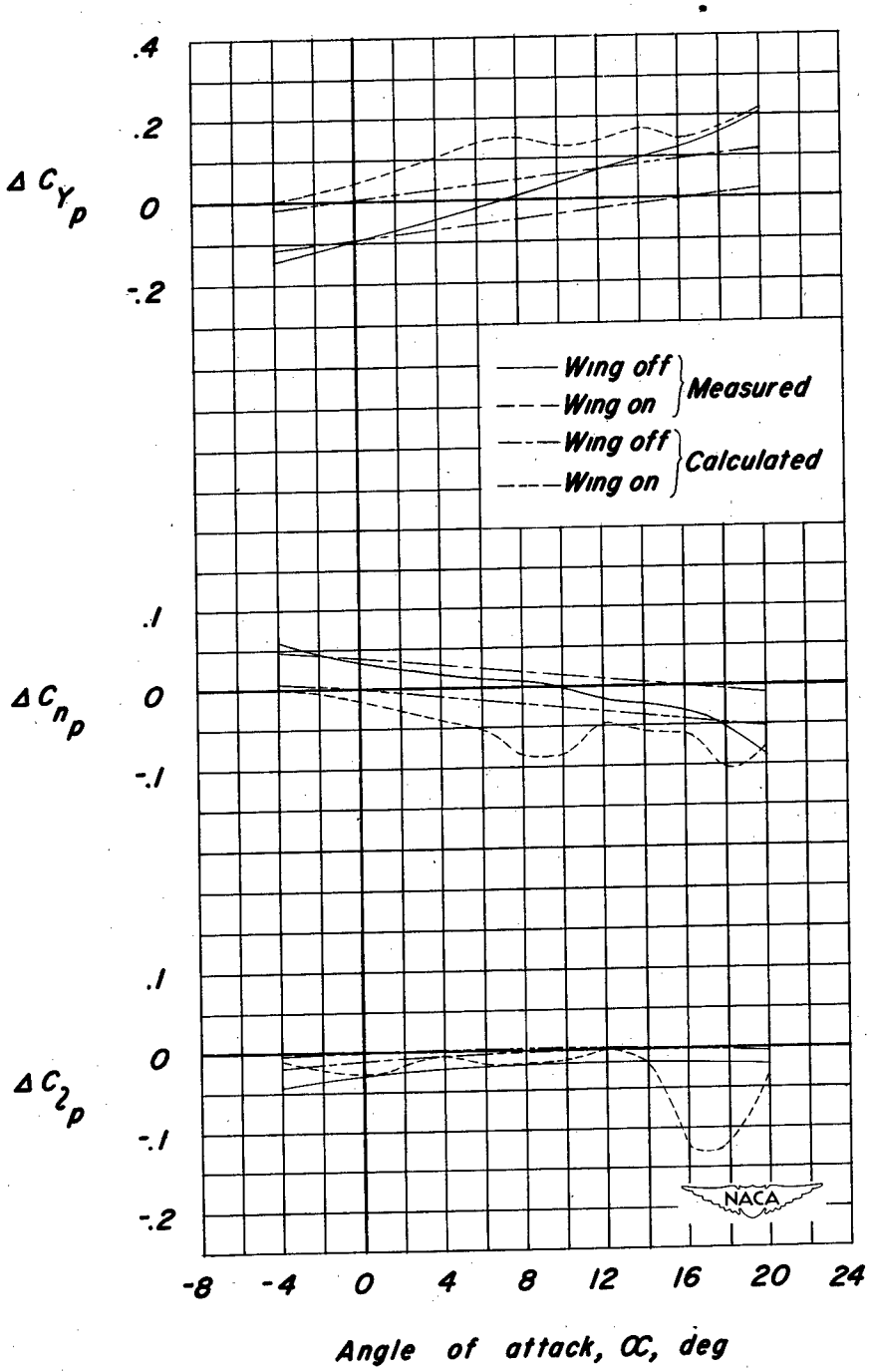

(c) High horizontal tail.

Figure 15.- Concluded.

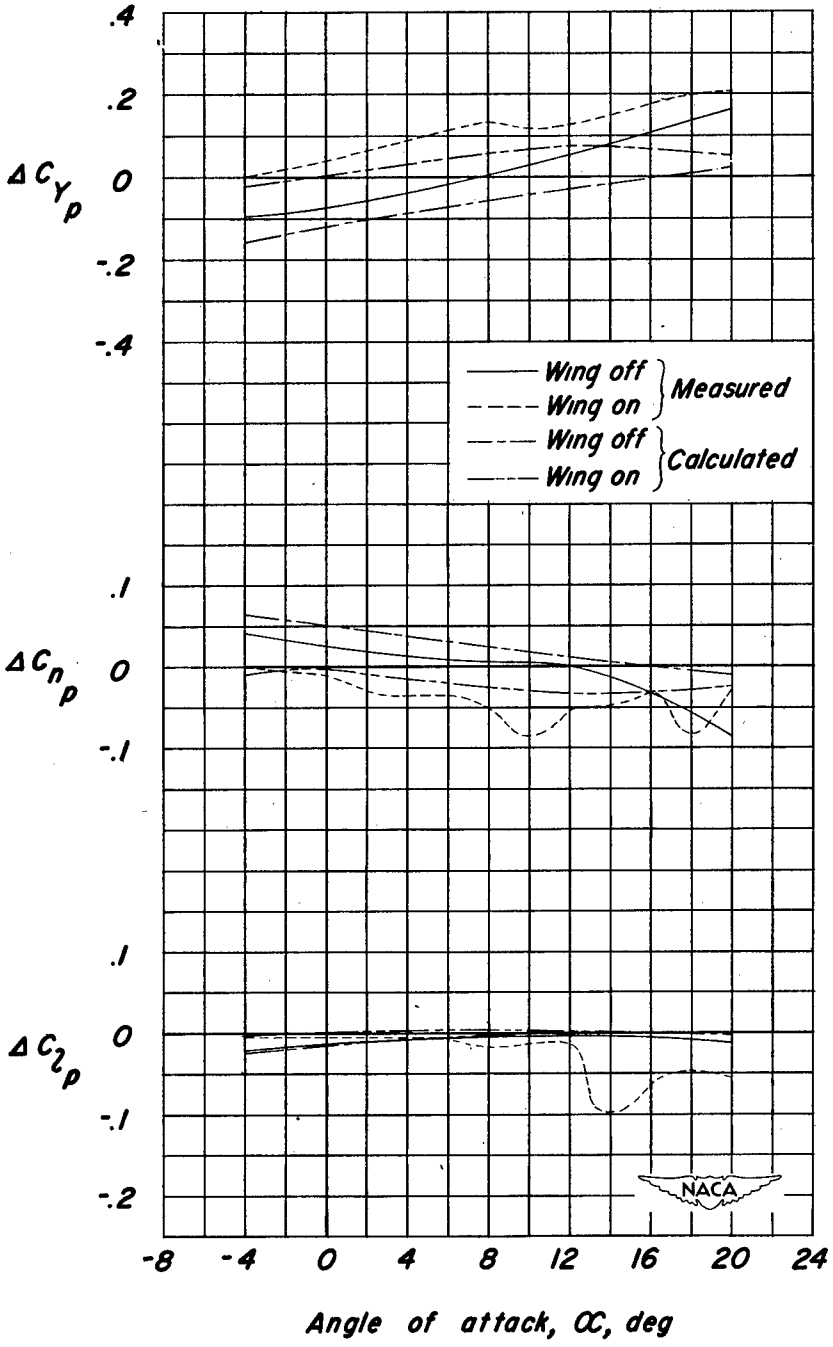

(a) Horizontal tail off.

Figure 16.- Comparison of the measured and calculated variation with angle of attack of the tail contributions ΔC_{Y_p}, ΔC_{n_p}, and ΔC_{l_p} for the model with wing on and wing off. Calculations based on measured ΔC_{Y_ψ}.

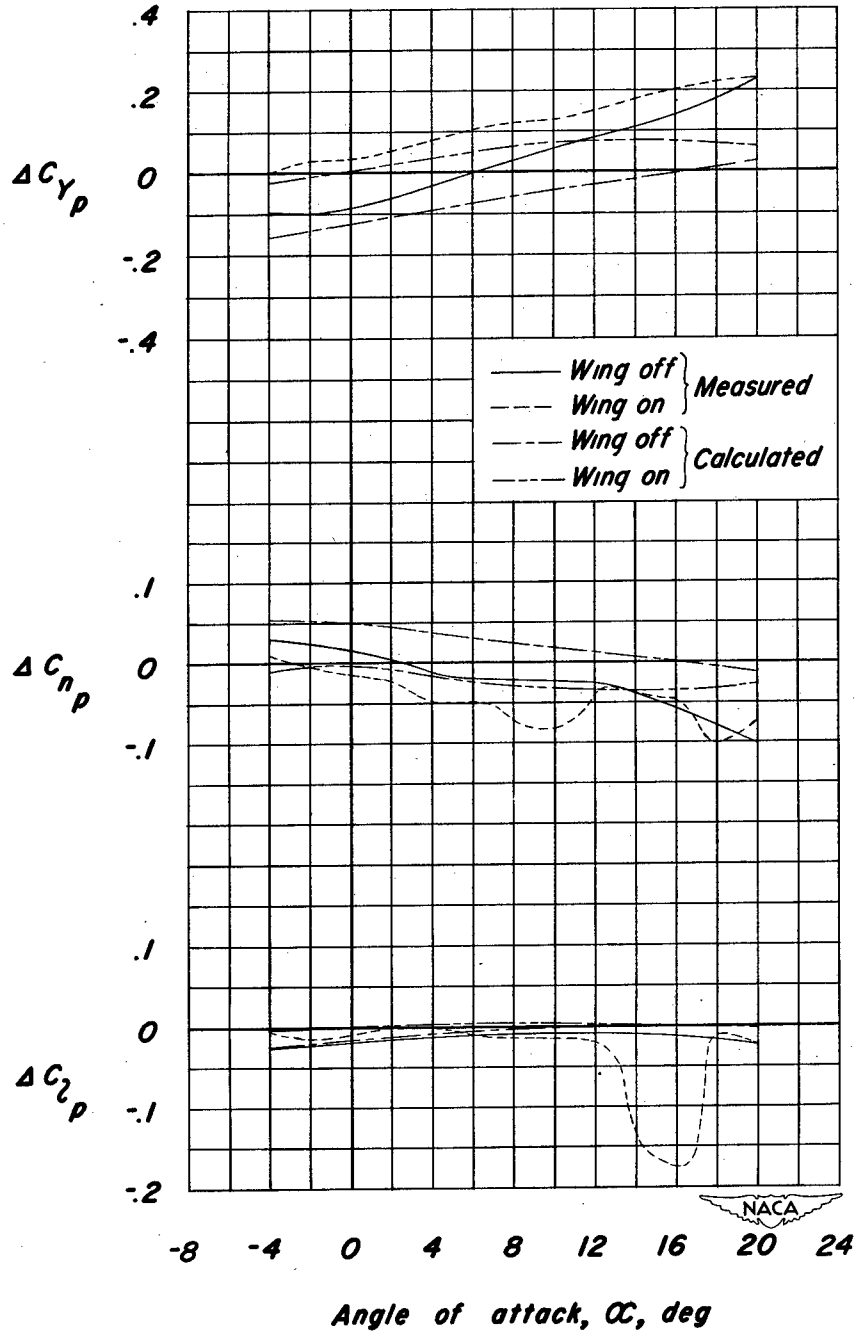

(b) Low horizontal tail.

Figure 16.- Continued.

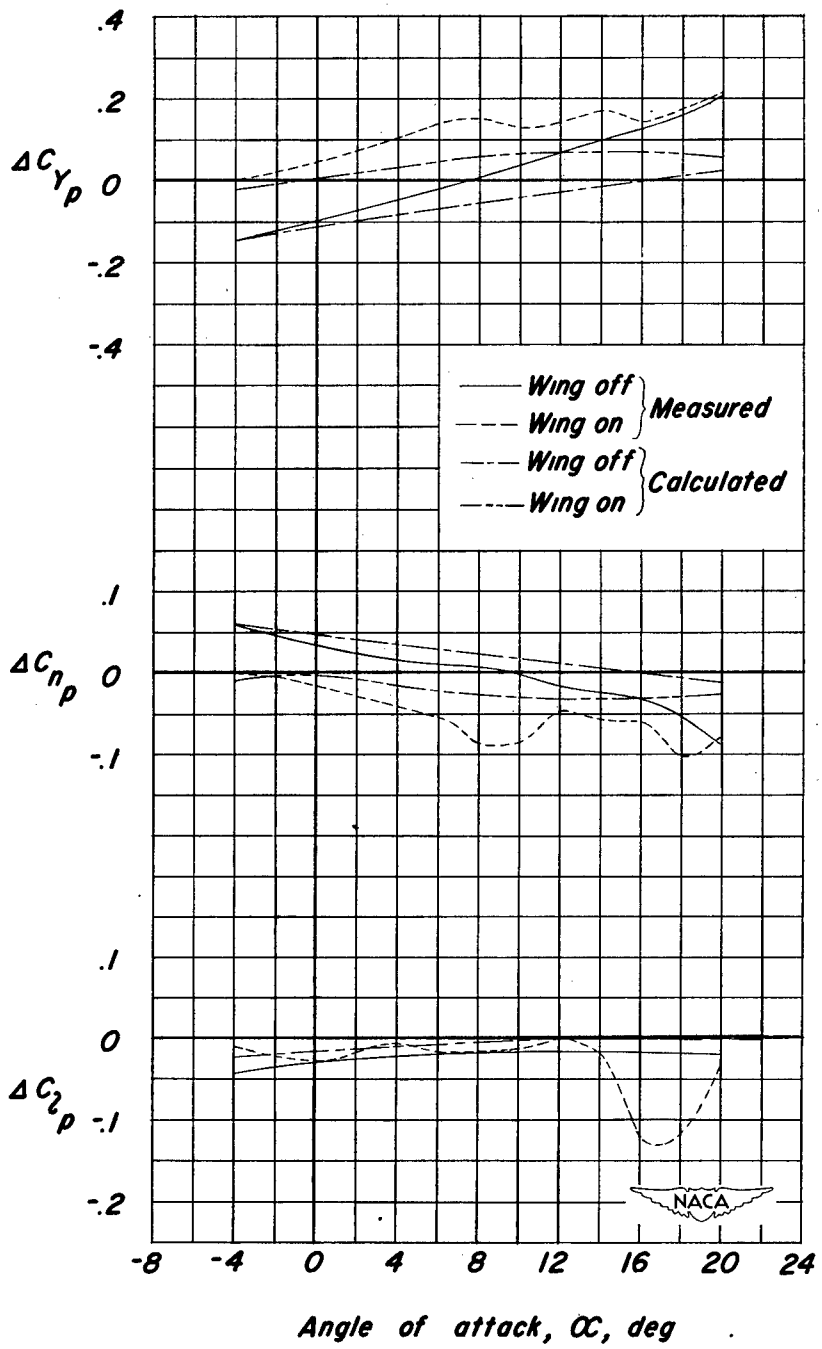

(c) High horizontal tail.

Figure 16.- Concluded.